JOURNAL OF GEOPHYSICAL RESEARCH, VOL. 114, D02306, doi:10.1029/2008JD010543, 2009

Columnar water vapor retrievals from multifilter rotating shadowband radiometer data

Mikhail D. Alexandrov,[1] Beat Schmid,[2] David D. Turner,[3] Brian Cairns,[4] Valdar Oinas,[5] Andrew A. Lacis,[4] Seth I. Gutman,[6] Ed R. Westwater,[7] Alexander Smirnov,[8] and James Eilers[9]

Received 4 June 2008; revised 24 October 2008; accepted 5 November 2008; published 24 January 2009.

[1] The multifilter rotating shadowband radiometer (MFRSR) measures direct and diffuse irradiances in the visible and near-infrared spectral range. In addition to characteristics of atmospheric aerosols, MFRSR data also allow retrieval of precipitable water vapor (PWV) column amounts, which are determined from the direct normal irradiances in the 940-nm spectral channel. The HITRAN 2004 spectral database was used in our retrievals to model the water vapor absorption. We present a detailed error analysis describing the influence of uncertainties in instrument calibration and spectral response, as well as those in available spectral databases, on the retrieval results. The results of our PWV retrievals from the Southern Great Plains (SGP) site operated by the Department of Energy (DOE) Atmospheric Radiation Measurement (ARM) Program were compared with correlative standard measurements by microwave radiometers (MWRs) and a global positioning system (GPS) water vapor sensor, as well as with retrievals from other solar radiometers (AERONET's CIMEL, AATS-6). Some of these data are routinely available at the SGP's Central Facility; however, we also used measurements from a wider array of instrumentations deployed at this site during the water vapor intensive observation period (WVIOP2000) in September–October 2000. The WVIOP data show better agreement between different solar radiometers or between different microwave radiometers (both groups showing relative biases within 4%) than between these two groups of instruments, with MWR values being consistently higher (up to 14%) than those from solar instruments (especially in the large PWV column amount range). We also demonstrate the feasibility of using MFRSR network data for creation of 2D data sets comparable with that of the MODIS satellite water vapor product.

Citation: Alexandrov, M. D., B. Schmid, D. D. Turner, B. Cairns, V. Oinas, A. A. Lacis, S. I. Gutman, E. R. Westwater, A. Smirnov, and J. Eilers (2009), Columnar water vapor retrievals from multifilter rotating shadowband radiometer data, *J. Geophys. Res.*, *114*, D02306, doi:10.1029/2008JD010543.

1. Introduction

[2] Water vapor (WV) is an important atmospheric component, influencing the Earth climate in many ways. Besides being a major greenhouse gas, it is also involved in aerosol growth. The global distribution of WV fields can be assessed only from satellite measurements. Currently WV data are acquired by a number of satellite sensors (both operational and research) such as the Moderate Resolution Imaging Spectroradiometer (MODIS [*Kaufman et al.*, 1997]) on NASA Aqua and Terra platforms, the Atmospheric Infrared Sounder (AIRS [*Aumann et al.*, 2003]) on Aqua, and the Tropospheric Emission Spectrometer (TES [*Beer*, 2006]) on NASA Aura. However, validation of the satellite products (which are affected by e.g., uncertainties in surface reflectivity) remains a critical problem. To address this problem a range of ground-based measurements are available worldwide, including radiosondes, Sun photometers, lidars, microwave radiometers (MWRs), and global

[1]Department of Applied Physics and Applied Mathematics, Columbia University and NASA Goddard Institute for Space Studies, New York, New York, USA.
[2]Atmospheric Science and Global Change Division, Pacific Northwest National Laboratory, Richland, Washington, USA.
[3]Space Science and Engineering Center, University of Wisconsin, Madison, Wisconsin, USA.
[4]NASA Goddard Institute for Space Studies, New York, New York, USA.
[5]Sigma Space Partners LLC and NASA Goddard Institute for Space Studies, New York, New York, USA.
[6]NOAA Earth System Research Laboratory, Boulder, Colorado, USA.
[7]NOAA-CU Center for Environmental Technology and Cooperative Institute for Research in Environmental Science, Department of Electrical and Computer Engineering, University of Colorado, Boulder, Colorado, USA.
[8]Science Systems and Applications, Inc. and NASA Goddard Space Flight Center, Greenbelt, Maryland, USA.
[9]NASA Ames Research Center, Moffett Field, California, USA.

0148-0227/09/2008JD010543$09.00

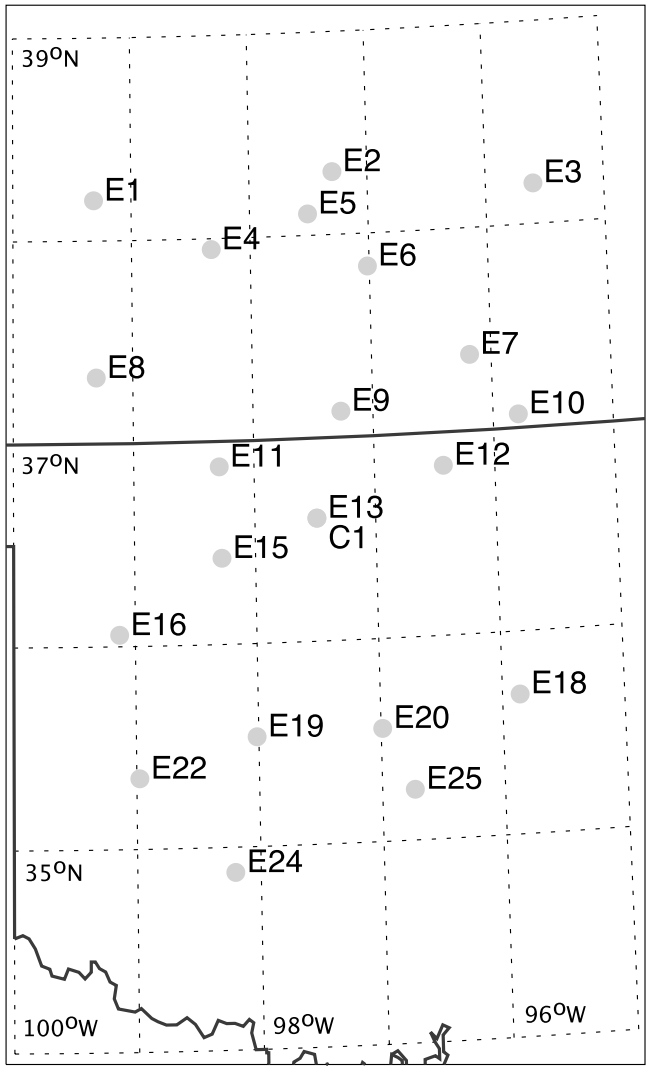

Figure 1. Locations of MFRSRs at the DOE ARM program ACRF site in the Southern Great Plains (SGP). The location of the Extended Facility E13 coincides with C1 at the Central Facility.

positioning system (GPS) receivers. Especially valuable are validations performed at measurement ''supersites'' such as the Southern Great Plains (SGP) site operated by the Department of Energy (DOE) Atmospheric Radiation Measurement (ARM) Program [*Ackerman and Stokes*, 2003], where multiple instrument types are available [*Tobin et al.*, 2006].

[3] The multifilter rotating shadowband radiometer (MFRSR [cf. *Harrison et al.*, 1994]) is one of the Sun photometer types deployed at the SGP site. The SGP MFRSR network consists of 21 instruments (Figure 1) located at SGP's Central and Extended Facilities (EFs) and covers the area of approximately 3 by 4 degrees in northern Oklahoma and southern Kansas with average spacing of 80 km between neighboring measurement sites. Besides the DOE ARM Program, the other major programs running MFRSR networks in the U.S. include the USDA UV-B Monitoring and Research Program [*Bigelow et al.*, 1998], the NOAA Surface Radiation (SURFRAD) Network [*Augustine et al.*, 2005], and the NASA Solar Irradiance Research Network (SIRN). Internationally, MFRSRs are operated mostly by individual users, however, many stations of the World Climate Research Programme (WCRP) Baseline Surface Radiation Network (BSRN) [*Ohmura et al.*, 1998] and the Australian Bureau of Meteorology Solar and Terrestrial Network [*Mitchell and Forgan*, 2003] are equipped with these instruments. The MFRSR measurements constitute a valuable, however yet underutilized, global data set.

[4] The MFRSR makes precise simultaneous measurements of the solar irradiances at six wavelengths (nominally 415, 500, 615, 673, 870, and 940 nm) at short intervals (20 sec for ARM instruments) throughout the day. Time series of direct solar beam extinctions and horizontal diffuse fluxes are derived from these measurements. Besides water vapor at 940 nm, the other gaseous absorbers within the MFRSR channels are NO_2 (at 415, 500, and 615 nm) and O_3 (at 500, 615, and 670 nm). Aerosols and Rayleigh scattering contribute atmospheric extinction in all MFRSR channels. Our recently updated analysis algorithm for MFRSR data [*Alexandrov et al.*, 2008] allows us to partition the spectral aerosol optical depth (AOD) into fine and coarse mode AODs and to retrieve the fine mode effective radius. Cloud screening is performed according to *Alexandrov et al.* [2004a]. After subtraction of the aerosol and Rayleigh contributions the optical depth in 940-nm channel is used for precipitable water vapor (PWV) retrievals described below.

[5] Sun-photometric PWV retrievals from the 940 nm water vapor absorption band have a long history dating back to works of *Fowle* [1912, 1915] (cf. *Thome et al.* [1992] for a brief history of the subject). In recent years a significant number of papers have been published describing PWV retrievals by means of ground-based Sun photometry [*Reagan et al.*, 1987a, 1987b, 1995; *Bruegge et al.*, 1992; *Thome et al.*, 1992, 1994; *Michalsky et al.*, 1995, 2001b; *Schmid et al.*, 1996, 2001; *Shiobara et al.*, 1996; *Halthore et al.*, 1997; *Cachorro et al.*, 1998; *Plana-Fattori et al.*, 1998, 2004; *Ingold et al.*, 2000; *Kiedron et al.*, 2001, 2003]. Recent retrievals of PWV from airborne Sun photometers have been reported by *Schmid et al.* [2003] and *Livingston et al.* [2007] (see references to earlier studies therein). Some of these studies were performed using shadowband radiometers such as MFRSR [*Michalsky et al.*, 1995, 2001b; *Schmid et al.*, 2001; *Plana-Fattori et al.*, 2004] and its more sophisticated relative Rotating Shadowband Spectroradiometer (RSS) [*Michalsky et al.*, 2001b; *Schmid et al.*, 2001; *Kiedron et al.*, 2001, 2003].

[6] We present a detailed error analysis describing the influence of measurement and modeling uncertainties, which may limit accuracy of Sun-photometric PWV retrievals. These factors include uncertainties in instrument calibration, laboratory-measured spectral filter profiles, and WV absorption line parameters in spectral databases (e.g., HITRAN [cf. *Rothman et al.*, 2005]). The latter problem has received attention in the recent years after the report of *Giver et al.* [2000] of errors in the widely used HITRAN 1996 database. Correction of these errors resulted in 14.4% increase of the line strength in the 940 nm absorption band. Shortly after that, a series of reports [*Belmiloud et al.*, 2000;

Schermaul et al., 2001a, 2001b] suggested a further 6% line strength increase in this band. At present the values of absorption parameters in this database appear to have stabilized, since the two most recent versions of HITRAN (2000 and 2004, including the 2006 upgrade of the latter [*Gordon et al.*, 2007]) show little difference, suggesting that HITRAN 2004 [*Rothman et al.*, 2005] is sufficiently accurate for use in PWV retrievals.

[7] While the accuracy of PWV measurements by solar transmittance (Sun-photometric) methods is not expected to be as good as that of standard instrumentation, such as microwave radiometers, Sun-photometric networks like AERONET [*Holben et al.*, 1998] and MFRSR networks mentioned above provide much better spatial coverage in a wider range of geographical locations. We will demonstrate the feasibility of deriving 2D maps from the particularly dense SGP MFRSR network data set, which characterizes spatial variability of PWV at given time and is comparable with the MODIS satellite product.

[8] Our PWV retrieval algorithm was applied to a year-long (2000) data set from the local MFRSR network at the SGP ARM Program site. The SGP's Central Facility (CF) contains two collocated MFRSRs (C1, E13). We present intercomparison between PWV column amounts derived from these instruments as a retrieval consistency check. We also present results of comparisons between MFRSRs and other sensors deployed at SGP's CF, such as AERONET's CIMEL Sun photometer, the C1 microwave radiometer (MWR), and a GPS receiver installed at the LMNO2 site of the NOAA Profiler Network (NPN [cf. *Wolfe and Gutman*, 2000; *Gutman et al.*, 2004], formerly called the Wind Profiler Demo Network (WPDN)), which is located about 9.5 km north of the SGP CF. In addition to these measurements routinely available throughout the year, we also used in our intercomparisons data from additional instruments (one Sun photometer and two MWRs) deployed at SGP's CF during the water vapor intensive observation period (WVIOP2000) from 18 September to 8 October 2000.

2. Retrieval Algorithm

[9] Sun-photometric measurements of direct normal irradiances in the 940 nm absorption band can be used for retrieval of PWV column amounts [*Michalsky et al.*, 1995; *Ingold et al.*, 2000; *Schmid et al.*, 2001; *Kiedron et al.*, 2001]. Our retrieval method for MFRSR data is based on inversion of the curve of growth relating the 940 nm slant optical depth of PWV

$$\tau_w^{(sl)} = m_w\,\tau_w = \tau_t^{(sl)} - m_a(\tau_R + \tau_a) \tag{1}$$

to the slant PWV column

$$u^{(sl)} = m_w u. \tag{2}$$

Here u is the vertical PWV column, m_w and m_a are the air masses for respectively WV [*Kasten*, 1965] and air [*Kasten and Young*, 1989], both depending on solar zenith angle (see *Kiedron et al.* [2001] for analysis of the air mass influence), $\tau_t^{(sl)}$ is the total slant optical depth (OD) in the 940-nm channel, τ_w is the optical depth of PWV, τ_R is the Rayleigh optical depth [*Hansen and Travis*, 1974]. τ_a is the aerosol optical depth (AOD) determined using Mie theory applied to the aerosol parameters derived from the data in the first five MFRSR channels according to *Alexandrov et al.* [2008]. The total WV transmittance $T_w^{(f)}$ for a particular instrument is computed by integration over wavelength λ of WV spectral transmittance $T_w(\lambda, u^{(sl)})$ (computed using a spectral database, e.g., HITRAN, for a standard atmospheric profile) with the laboratory-measured spectral response function (SRF) $f(\lambda)$ of the 940-nm channel filter. The integration is weighted with the (nominal) TOA solar irradiance $I_0(\lambda)$.

$$T_w^{(f)}\left(u^{(sl)}\right) = \frac{\int_{\lambda_1}^{\lambda_2} T_w\left(\lambda, u^{(sl)}\right) f(\lambda) I_0(\lambda)\,\mathrm{d}\lambda}{\int_{\lambda_1}^{\lambda_2} f(\lambda) I_0(\lambda)\,\mathrm{d}\lambda}, \tag{3}$$

and the curve of growth is defined as the dependence of

$$\tau_w^{(sl)} = -\ln T_w^{(f)} \tag{4}$$

on $u^{(sl)}$.

[10] To compute the curves of growth for our retrieval algorithm we use HITRAN 2004 spectral absorption database together with NASA GISS LBL3 line-by-line radiative transfer code (briefly described by *Lacis and Oinas* [1991]). A comprehensive intercomparison study [*Collins et al.*, 2006] showed an excellent agreement between this code and other line-by-line codes used by scientific community. This code uses the water vapor continuum by *Tipping and Ma* [1995] for wavelengths larger than 1 μm, while the continuum absorption at shorter wavelengths (including the 940 nm band) is neglected.

[11] An example of MFRSR SRF (head 922, deployed on the C1 MFRSR during the year 2000) is shown in Figure 2 (top). It is normalized to unity at the response's maximum and is plotted over the spectral transmittance of PWV corresponding to 1 cm column and computed using HITRAN 2004 database. Examples of curves of growth computed for this SRF using various spectral absorption databases (three versions of HITRAN and the European Space Agency ESA-WVR database) are shown in Figure 2 (bottom). This plot also shows an empirical curve of growth relating MFRSR-derived slant WV optical depths to the correlative PWV column measurements by the C1 MWR.

[12] Usually the curve of growth can be closely approximated by a power law function [*Moskalenko*, 1969; *Pitts et al.*, 1974, 1977; *Koepke and Quenzel*, 1978; *Bruegge et al.*, 1992]

$$\tau_w^{(sl)} \approx a(mu)^b, \tag{5}$$

with a and $b \approx 0.6$ being adjustable parameters (here and in the rest of the paper we drop the subscript of m_w). Some authors [e.g., *Gates and Harrop*, 1963; *Reagan et al.*, 1987a, 1987b] use more restrictive approximation with the theoretical value $b = 1/2$ ("square root law" [cf. *Goody*, 1964]). Both these parameterizations are not very accurate at large air masses [*Schmid et al.*, 2001], thus, we use the

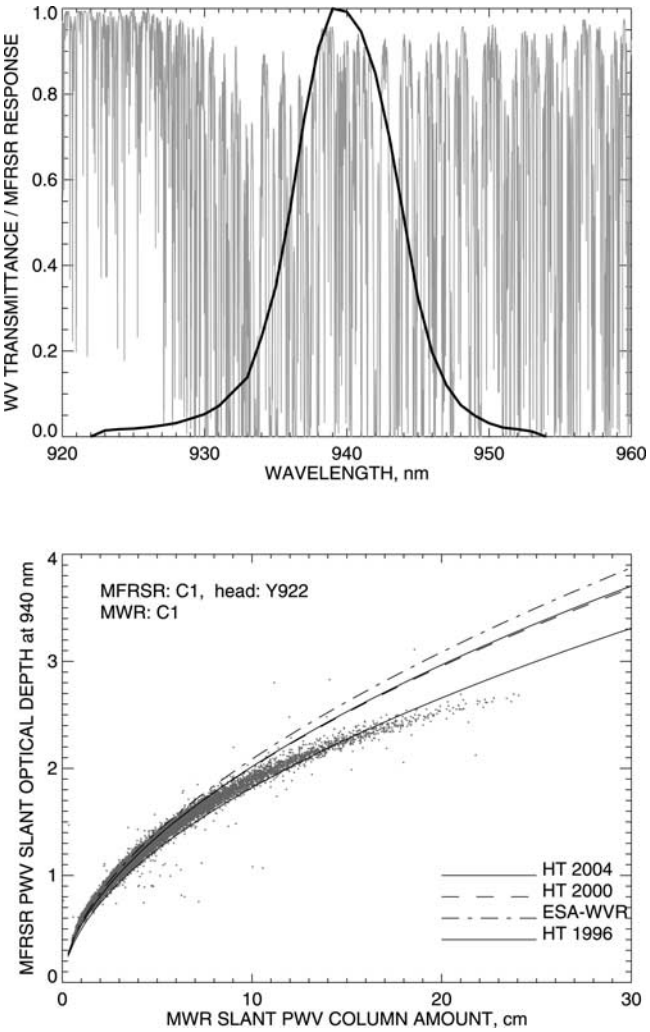

Figure 2. (top) Spectral transmittance of WV corresponding to a 1-cm column amount computed using the HITRAN 2004 database (gray) and the MFRSR (head 922) 940-nm channel spectral response function normalized to unity at the maximum (black). (bottom) Experimental curve of growth constructed by plotting MFRSR-derived slant optical depth in 940-nm channel (with AOD and Rayleigh subtracted) versus MWR-derived slant PWV column (data from SGP CF, 2000). The curves of growth obtained by integrating MFRSR spectral response functions with WV absorption spectra from various databases (HITRAN 1996, 2000, and 2004, and ESA-WVR) are shown by lines.

actual curves of growth in our inversions. However, the simple form of equation (5) makes it a useful tool for estimation of retrieval uncertainties presented in the next Section.

3. Measurement and Retrieval Uncertainties

[13] As for any retrieval from a radiometric measurement, accurate determination of PWV column requires sufficient characterization of the sensor (spectral response, calibration) and adequate modeling assumptions (spectral absorption database, correction for aerosol and Rayleigh scattering). The PWV retrieval process consists of two stages. First, we need to determine WV optical depth τ_w by subtracting aerosol and Rayleigh ODs from calibrated total optical depth in 940-nm channel. In the second stage we use the curve of growth (4) to translate this τ_w into the corresponding PWV column amount. Both these stages, as well as calibration, may produce errors, which then are propagated into the final column PWV result.

[14] To show how an error in τ_w affects the retrievals, let us use the approximate curve of growth formula (5). In this case an error in (vertical, not slant) PWV OD $\delta\tau \ll \tau_w$ results in the corresponding error in PWV column.

$$\delta u = \frac{(mu)^{1-b}}{ab}\delta\tau + \frac{1-b}{2(ab)^2}m^{2-2b}u^{1-2b}(\delta\tau)^2 + \ldots \qquad (6)$$

Note, that if $b = 1/2$ this series expansion is finite and the second term does not depend on u

$$\delta u = 2\frac{\sqrt{mu}}{a}\delta\tau + \frac{m}{a^2}(\delta\tau)^2. \qquad (7)$$

We should note, that in any realistic situation ($a \approx 0.5$, $b \approx 0.5$, $\delta\tau \leq 0.05$, $u > 0.01$ cm) the second term in (6) and (7) is infinitesimally small (less than 0.01 cm) and can be omitted, thus

$$\delta u = \frac{(mu)^{1-b}}{ab}\delta\tau = \frac{1}{ab}\left(\frac{u}{\mu}\right)^{1-b}\delta\tau, \qquad (8)$$

where $\mu \approx \cos\theta$ is the inverse air mass (θ is the solar zenith angle). This formula can be applied to errors of any nature including calibration uncertainties and artifacts induced by various technical problems, such as e.g., inadequate angular response characterization and/or instrument tilt [cf. *Alexandrov et al.*, 2007]. Note, that while angular response error does not have a specific spectral signature, instrument tilt induces the same artificial OD variation in all MFRSR channels. Being spectrally flat, this variation is likely to be attributed to coarse mode AOD and, therefore, has little influence on PWV retrievals.

[15] Another major uncertainty of PWV retrievals from solar radiometer data is related to limited accuracy of determination of the instrument's curve of growth (4), or parameters a and b in the approximation (5). This uncertainty combines effects of imperfect instrument's spectral response characterization and possible errors in the WV spectral absorption databases. To show the influence of this uncertainty on the retrieved PWV column, we use (5) with true values of a and b to obtain the slant OD from the PWV column u, and then derive an erroneous column u' using the same equation with incorrect parameters a' and b'.

$$m\tau_w = a(mu)^b = a'(mu')^{b'}. \qquad (9)$$

It follows from here that

$$u' = \left(\frac{a}{a'}\right)^{1/b'} m^{b/b'-1}u^{b/b'}, \qquad (10)$$

or equivalently

$$\frac{u'}{u} = \left(\frac{a}{a'}\right)^{1/b'} (mu)^{b/b'-1}. \quad (11)$$

We see in equation (10) a combination of an overall scale factor, an artificial diurnal variation (with air mass m), and a nonlinear transformation of the PWV column amount u. Note, that the first factor reflects mainly change in a (given $b' \approx b$), while the last two factors are induced by changes in b only (they become trivial if $b' = b$). Below we will compare magnitudes of these factors using the real MFRSR SRFs and different spectral absorption databases. We should note, that when the errors in a and b are small (i.e., $a' \approx a$ and $b' \approx b$) the resulting error in PWV content can be also estimated using equation (8) with $\delta\tau = a'(mu)^{b'} - a(mu)^b$ (here a and b are nominal parameters, while a' and b' are actual ones). In this situation we consider the nominal parameters as the "true", and the difference between actual and nominal curves of growth as an error in measured optical depth. The result of this computation is consistent with equation (11).

3.1. Instrument Calibration

[16] The power law parameterization (5) is used in the "modified Langley plot" calibration technique [*Reagan et al.*, 1987a, 1987b; *Bruegge et al.*, 1992]. This technique is similar to the standard Langley analysis, however, instead of relative stability of AOD at large zenith angles, it requires stability of PWV column, which rarely occurs in reality (except for very dry places like the Arctic [*Kiedron et al.*, 2001] or high mountains [*Schmid et al.*, 1998]). In all other cases this technique can provide only rough characterization of instrument's responsivity [cf. *Michalsky et al.*, 2001b] and can even introduce large calibration errors. Because of this, we rely on laboratory calibration of the 940 nm MFRSR channel in our data analysis. We should emphasize the necessity of frequent calibration checks and corrections, since some MFRSR filters may experience rapid sensitivity loss (e.g., *Alexandrov et al.* [2002] reported the loss of filter transmittance approximately by a factor of 3 for MFRSR's 615-nm and 670-nm channels during the first 200 days of instrument operation, followed by gradual stabilization).

[17] In the laboratory lamp calibration process the output of the radiometer V_L (in volts or counts) is measured when the instrument is illuminated by a standard lamp with known spectral irradiance $I_L(\lambda)$. Then the instrument's responsivity (calibration constant) R in a given spectral channel is determined from the relation

$$V_L = R \int I_L(\lambda) f(\lambda) \mathrm{d}\lambda, \quad (12)$$

where f is the known (or assumed to be known) spectral response function of the instrument in this channel. This calibration constant is then used to convert the output V of a field measurement into the irradiance transmitted through the atmosphere

$$I^{(f)} = \frac{V}{R}. \quad (13)$$

In our analysis we use calibrated 940-nm channel irradiances (13) from the standard ARM data product. These irradiances are computed using calibration constants supplied by the instrument manufacturer. Then, we use our extraterrestrial spectral solar flux data to convert these irradiances into the total optical depths to be analyzed. To do this we represent the measured value (13) as

$$I^{(f)} = \int T_t(\lambda) I_0(\lambda) f(\lambda) \mathrm{d}\lambda = I_0^{(f)} T_t^{(f)}, \quad (14)$$

where $T_t(\lambda)$ is the total spectral atmospheric transmittance, $I_0(\lambda)$ is the TOA solar irradiance,

$$I_0^{(f)} = \int I_0(\lambda) f(\lambda) \mathrm{d}\lambda \quad (15)$$

is the irradiance, which would be measured by the instrument at the top of the atmosphere, and

$$T_t^{(f)} = \frac{\int T_t(\lambda) I_0(\lambda) f(\lambda) \mathrm{d}\lambda}{\int I_0(\lambda) f(\lambda) \mathrm{d}\lambda} \quad (16)$$

is the total atmospheric transmittance in the instrument's channel, which is then converted into the total slant optical depth

$$\tau_t^{(sl)} = -\ln T_t^{(f)}. \quad (17)$$

[18] In the case of calibration uncertainty, the error in (vertical) OD has the form [*Alexandrov et al.*, 2002, 2007]

$$\delta\tau = c\ \mu = \frac{c}{m}, \quad (18)$$

where c is a constant. In a curve of growth plot (as in Figure 2) addition of calibration (18) shows up as a vertical shift by c. Substitution of (18) into (8) results in

$$\delta u = \frac{1}{ab} \frac{u^{1-b}}{m^b}\ c = \frac{1}{ab} u^{1-b} \mu^b\ c \quad (19)$$

which has the following simple form for $b = 1/2$.

$$\delta u = \frac{2}{a} \sqrt{\frac{u}{m}}\, c = \frac{2}{a} \sqrt{u\mu}\, c \quad (20)$$

We see from (19), (20) that δu (as $\delta\tau$) is maximal at noon.

[19] Laboratory (lamp) calibrations of MFRSRs (and other Sun photometers) have accuracy of 2–4% [*Michalsky et al.*, 2001a; *Kiedron et al.*, 1999; *Schmid et al.*, 1998]. The errors come from both inaccuracy of calibration transfer from primary standards and uncertainties in knowledge of the extraterrestrial spectral irradiance [*Harrison et al.*, 2003; *Schmid et al.*, 1998]. In our retrievals we use the American Society for Testing and Materials AM 0 reference Solar spectrum (ASTM E-490, available at http://rredc.nrel.gov/solar/spectra/am0/) developed in 2000. Note, that some older spectra [e.g., *Kneizys et al.*, 1988] may be "WV contaminated", when atmospheric WV absorption was not completely removed from the spectrum resulting in lower

TOA irradiance. This may result in up to 5% calibration error. The lamp calibration accuracy of 2–4% translates into a possible calibration error with c between 0.02 and 0.04. The HITRAN 2004 curve of growth for the MFRSR head 922 (Figure 2, bottom) can be approximated by expression (5) with $a = 0.55$ and $b = 0.56$. For these parameters we can estimate the magnitude of a possible calibration error. For SGP's CF μ at noon varies from 0.5 in winter to $0.97 \approx 1$ in summer. As it is seen from Figure 4, the typical PWV column at this site also has a seasonal variation with a winter minimum of 0.5 cm and a summer maximum of around 4 cm. Using equation (19) we can estimate that for the instrument characteristics listed above and a calibration error with $c = 0.03$, the error induced in the PWV column will be 0.05 cm (10%) in winter and 0.18 cm (4.5%) in summer. Note, that while the absolute error is larger in summer (with larger PWV amounts and smaller air masses) than in winter, the corresponding relative error is smaller.

[20] Given a standard PWV measurements (e.g., by a collocated MWR), the relation (19) allows one to investigate whether the error in MFRSR-derived PWV column is induced by calibration uncertainties. This can be done by computing the time series of the calibration coefficient values

$$c = ab\, m^b\, u_{MWR}^{b-1}(u_{MFR} - u_{MWR}) \tag{21}$$

and check if it is indeed constant during the day. If it is, this value of c can be used to correct the Sun photometer calibration. The same test can be performed graphically by checking if the empirical (MWR–MFRSR) curve of growth in Figure 2 (bottom) can match the theoretical one (computed using a spectral absorption database) in the whole slant PWV column range after a vertical shift, that is, addition of a constant slant OD (the value of which will be c). We see, for example, that this is not the case in Figure 2 (bottom), thus, while a calibration error may affect the MFRSR measurements presented there, it is not, at least, the only source of uncertainty. To some extent, these procedures can be used to find a relative calibration difference between two collocated Sun photometers, however in this case the result may depend on which of them is chosen as the "standard" measurement source.

3.2. Correction for Aerosol and Rayleigh Scattering

[21] Rayleigh optical depth at 940 nm wavelength is really small (around 0.01 at standard 1013.25 mb pressure), thus any uncertainties of few percent (rather affecting the UV spectral region than NIR [cf. *Teillet*, 1990]) have practically negligible effect on PWV retrievals. We use retrievals of fine and coarse mode AOD and fine mode effective radius made according to *Alexandrov et al.* [2008] to compute AOD in the 940-nm channel by means of Mie theory. *Alexandrov et al.* [2008] presented results from SGP's CF MFRSRs for the year 2000 in comparison with AERONET's Sun-sky inversions from a collocated CIMEL Sun photometer. This comparison showed remarkably good agreement. The differences in total, fine and coarse mode AOD did not exceed the expected measurement accuracy of 0.01, while the retrieved values of fine mode effective radius showed no relative bias and only 0.03 μm random error (standard deviation of the differences). If only data with large enough AOD (more than 0.06 at 870 nm) are selected, the error in particle size is reduced by a factor of two, becoming about 10% of a typical fine mode effective radius value. This indicates robustness of the aerosol retrievals from MFRSR data. Small errors in aerosol retrievals come from calibration uncertainties and instrumental artifacts (e.g., tilt). The extrapolated coarse mode AOD in the 940-nm channel during the year 2000 was essentially the same as that at 870 nm wavelength (0.050 ± 0.031), while the fine mode AOD (0.027 ± 0.024) constituted 81 ± 2% of the corresponding 870 nm value (0.033 ± 0.029). The 2% standard deviation in the AOD ratio is caused by variation of the fine mode particle size. We assume that 870 nm AOD τ is known with the accuracy $\delta\tau$, both split into fine and coarse modes.

$$\tau + \delta\tau = (\tau_f + \delta\tau_f) + (\tau_c + \delta\tau_c). \tag{22}$$

This allows us to estimate the accuracy $\delta\tau'$ of AOD τ' at 940 nm using the relation

$$\tau' + \delta\tau' = (q + \delta q)(\tau_f + \delta\tau_f) + (\tau_c + \delta\tau_c), \tag{23}$$

where q is the spectral conversion factor and δq is its uncertainty (due to possible error in particle size retrieval). We assume (and this is supported by the comparison with AERONET mentioned above) that our fine mode particle size retrievals are unbiased, thus, the observed mean ratio of 0.81 between 940 and 870 nm fine mode AOD is a good estimate for q. We also assume that the random error in determination of q does not exceed its observed natural variability, thus, we accept the standard deviation of this variability as $\delta q = 0.02$. Retaining only the terms in (23), which are linear in "δ", we obtain the following estimate of uncertainty in extrapolation of 940 nm AOD.

$$\delta\tau' = \delta\tau + (q - 1)\delta\tau_f + \delta q\ \tau_f. \tag{24}$$

Here the first term reflects the uncertainty in total AOD outside the WV band (at 870 nm), the second term corresponds to a possible error in separation between fine and coarse mode AODs, and the third term is related to uncertainty in retrieval of fine mode particle size. Note, that the second term is zero in a hypothetical case $q = 1$, when either the two wavelengths are the same (thus, $\tau' = \tau$, $\delta q = 0$, and, therefore, $\delta\tau' = \delta\tau$), or the fine mode AOD has the same spectral signature as the coarse mode (thus, the two modes are indistinguishable, and any formal separation has no effect on the results). The results of *Alexandrov et al.* [2008] suggest that $\delta\tau_f \sim \delta\tau = 0.01$. This leads to the value of 0.002 for the second term in (24), which is negligible compared to $\delta\tau$. The fine mode AOD at 870 nm wavelength exhibited seasonal variability in 2000 with smaller values in winter (around 0.01) and larger values in summer (around 0.05–0.06) with the annual mean of 0.033 and standard deviation of 0.029. (The total AOD in this year had annual mean 0.082 and was dominated by the coarse mode AOD with the annual mean of 0.049). These data result in estimates of the third term in (24) between 0.0002 and 0.0012, which are an order of magnitude smaller than $\delta\tau$ and can be neglected. Thus we see that the estimate of AOD

in 940-nm channel depends only weakly on the aerosol model assumptions and is mostly determined by the accuracy of total AOD measurements. The 0.01 accuracy in extrapolated AOD translates by (8) into PWV column accuracy of 0.03 cm (6%) in winter and 0.06 cm (1.5%) in summer (at noon and under conditions described in section 3.1). These errors are 2–3 times smaller than calibration uncertainties.

3.3. Water Vapor Spectral Absorption Databases

[22] While the MFRSR response functions are not always accurately determined, problems affecting the PWV retrievals have been also related to uncertainties in spectral databases of water vapor absorption, as described in section 1. These uncertainties are illustrated in Figure 2 (bottom) by comparing of the curve of growths computed for MFRSR's head 922 using four different spectral databases: HITRAN 1996, 2000, 2004 [*Rothman et al.*, 2005] http://cfa-www.harvard.edu/hitran/) and European Space Agency's ESA-WVR database [*Schermaul et al.*, 2001a, 2001b] http://badc.nerc.ac.uk/data/esa-wv/). These curves differ quite significantly from each other and from the empirical curve obtained by plotting MFRSR-derived slant optical depth at 940 nm (with AOD and Rayleigh contribution subtracted) versus PWV slant column derived from collocated microwave radiometer measurements (C1 MWR, original ARM product). However, the two most recent databases, HITRAN 2000 and 2004 (with or without 2006 update described by *Gordon et al.* [2007]), yield almost identical results suggesting that perhaps the spectral databases have become more reliable, and HITRAN 2004 is suitable for accurate PWV retrievals.

[23] Let us use equation (10) to estimate the error from using HITRAN 1996, assuming that HITRAN 2004 correctly describes WV absorption. The HITRAN 2004 parameters in (5) for head 922 are $a = 0.55$ and $b = 0.56$. Both these parameters calculated using the older HITRAN 1996 are smaller: $a' = 0.51$ and $b' = 0.55$. Assuming that the true PWV column has value u, we use (10) to interpret the corresponding slant PWV OD in terms of HITRAN 1996 PWV column u'.

$$u' = 1.15\, m^{0.02} u^{1.02}. \tag{25}$$

We see from this relation, that the largest error, a 15% overestimation, comes from the overall factor. The second factor in (25) indicates a smaller additional increase in PWV column significant mostly at large air mass (dawn, dusk, winter season), and reaching 3.3% at $m = 5$. The last factor in (25) is noticeable at large PWV columns (2.8% at $u =$ 4 cm). *Schmid et al.* [2001] came to a similar conclusion, that the correction of the HITRAN 96 database according to *Giver et al.* [2000] (a 14.4% increase of the line strength for the 940 nm band) will decrease the PWV retrievals from the solar radiometers used in their study by 8–13%, and that a further decrease is expected if findings by *Belmiloud et al.* [2000] of additional 6% line strength increase are implemented (the latter study lead to ESA-WVR database addressed below). Note, that the HITRAN 1996 curve of growth in Figure 2 appears to be closer to the MFRSR–MWR observation-based dependence at large slant PWV amounts than the curve of growths derived using later versions of spectral absorption databases. This observation supports another conclusion of *Schmid et al.* [2001] that adoption of the newer spectral absorption data will increase disagreement of solar PWV measurements with MWR.

[24] As seen in Figure 2 (bottom), the differences in WV spectral absorption between HITRAN 2004, HITRAN 2000 and ESA-WVR databases are much smaller compared to these between 1996 and 2004 versions of HITRAN. The curve of growth parameters of (5) computed using HITRAN 2000 are practically the same as for HITRAN 2004 (differences in both a and b are as little as 0.001), thus, producing a negligible error of 0.35% in retrieved PWV column amount. The same is true for the 2006 update of HITRAN 2004 [*Gordon et al.*, 2007], which results in about 0.9% (underestimation) difference in retrievals compared to the original version. (Note, that differences of less than 1% are comparable to the accuracy of the approximation (5), thus, the exact difference values may be slightly different.) The disagreement between HITRAN 2004 and ESA-WVR is larger. Using ESA-WVR, we derive $a = 0.57$ and $b = 0.57$ for head 922, which lead to 5% underestimation of PWV column amount compared to HITRAN 2004. This value can be taken as an upper bound measure of the uncertainty associated with WV database accuracy. Note, however, that this estimate may be much larger than the actual error induced by uncertainties in spectral databases. The measurements and computations by *Brown et al.* [2002], on which the WV part of HITRAN 2000 is based, were made later than the work of *Schermaul et al.* [2001a, 2001b] and used more up-to-date line broadening data while measuring empirical intensities of 70% more lines in the 940 nm band. Another indication that HITRAN 2000 is more accurate in the 940-nm spectral region than ESA-WVR was provided by an independent study by *Tolchenov et al.* [2003], who reanalyzed the ESA-WVR linelist and concluded that the line intensities in it should be in fact closer to those of *Brown et al.* [2002]. From the measurement perspective, *Albert et al.* [2004] reported that using HITRAN 2000 instead of ESA-WVR in ground-based spectrometric PWV retrievals (in the 940 nm band) produced better agreement with correlative radiosonde data.

[25] The strength of the water vapor continuum absorption currently remains a subject of discussion in the scientific community. In particular, the CKD (Clough, Kneizys, and Davis) semiempirical continuum model [*Clough et al.*, 1989] and especially its recent versions like MT CKD (cf. *Clough et al.* [2005], *Vogelmann et al.* [1998], *Sierk et al.* [2004], and *Reichert et al.* [2007] for description and comparison with measurements) predict much stronger in-band continuum absorption than the theory of *Tipping and Ma* [1995]. As we indicated earlier in the paper, the GISS LBL3 code used for computation of our MFRSR curves of growth does not include the WV continuum absorption in the 940 nm band (while the *Tipping and Ma* [1995] continuum model is used for wavelengths larger than 1 μm). However, as we will show below, the MFRSR retrievals show no significant bias relative to the results from other solar radiometers (AATS-6, AERONET's CIMEL), which data analyses do account for WV continuum (AATS-6 analysis is based on the LBLRTM 5.21 radiative transfer code including CKD continuum model, while the AERONET's SHARM radiation code incorporates MT CKD model).

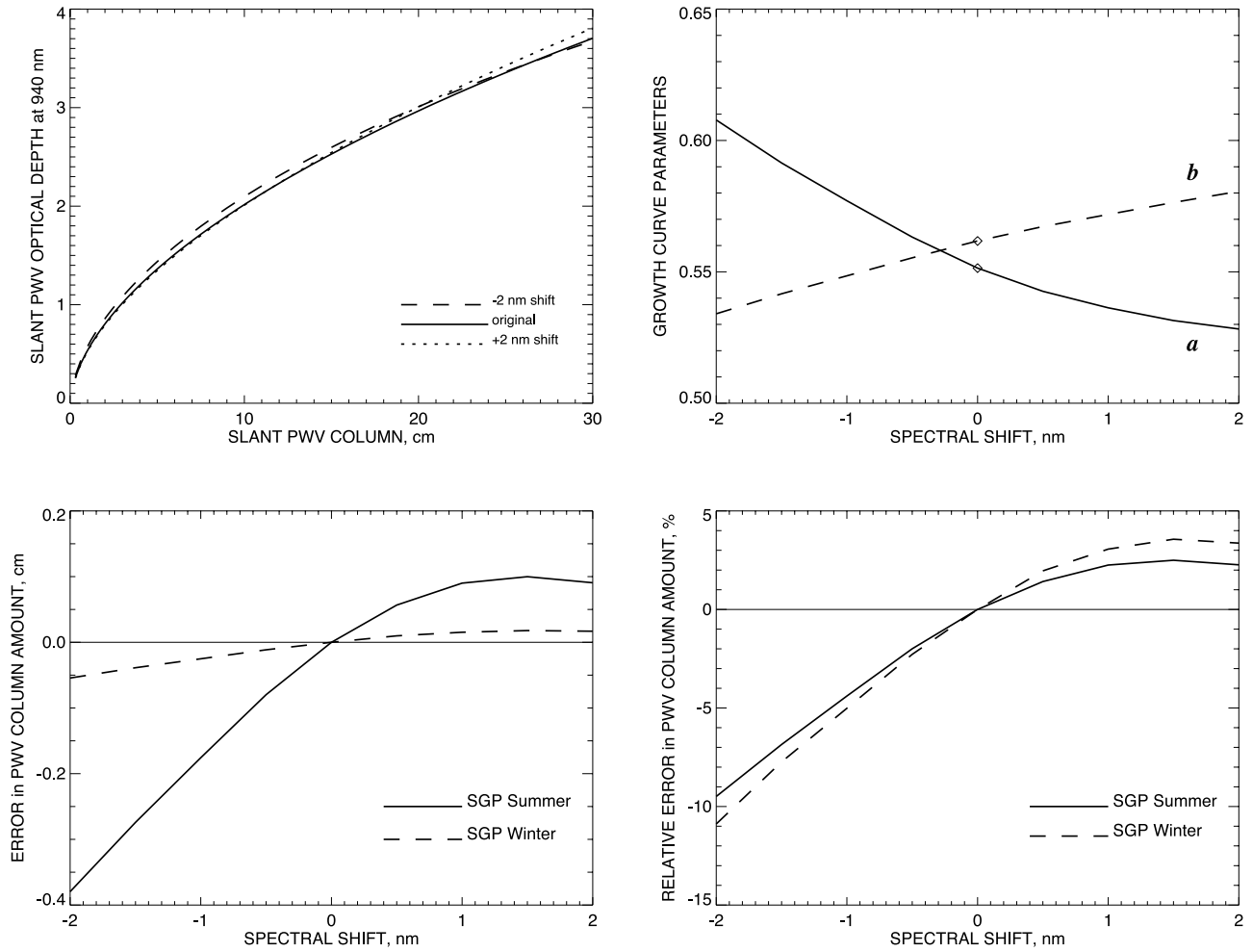

Figure 3. Effects of spectral shifts (up to ±2 nm) of the spectral response function for the MFRSR head 922 (Figure 2) on the curve of growth (computed with HITRAN 2004 spectral database). (top left) Comparison between the original and shifted curves of growth. (top right) Parameters a and b of equation (5) as functions of spectral shift (the original values are shown by diamonds). (bottom left) Absolute and (bottom right) relative errors in retrieved PWV column induced by the shifts for typical SGP conditions (winter: 0.5-cm PWV column, m = 2 [at noon]; summer: 4-cm PWV column, m = 1.03).

We can explain this agreement either by assuming that WV continuum absorption is negligibly weak, or rather by the difference in the way the different line-by-line (LBL) models perform computations. Each LBL model has a number of free parameters, governing, e.g., the rule of separation between the absorption line proper and its wings, as well as the assumed shape of the latter. In particular, despite both CKD and GISS LBL3 models use the same 25 cm^{-1} cutoff separating the line from its wings, they still have different definitions of the line and continuum absorption. In the CKD model the continuum is composed not only of the remaining of the line shape outside the 25 cm^{-1} window but also includes the so-called "pedestal" the constant residual absorption evaluated at 25 cm^{-1} from the line center. On the contrary, in the GISS model this "pedestal", which constitutes a significant part of the continuum in the CKD model, is attributed to the absorption of the line itself. We can point to a good graphical illustration of this difference in the paper by *Vogelmann et al.* [1998] (Figure 3). Here we see that the CKD model uses a horizontal cutoff separating the line and continuum absorption, while the dotted lines in this plot correspond to the 2 vertical cutoffs used in the GISS model. *Clough et al.* [1989] acknowledge this freedom of continuum definition (e.g., they cite works of D. E. Burch, who used vertical cutoffs, as we do) and explicitly state that "if a band model is to be used in conjunction with a continuum, then the absorption effects included in the continuum must be excluded from the band model". This difference in line-continuum separation may be sufficient to explain the good agreement of our MFRSR retrievals (with no continuum assumed) with the above mentioned retrievals from AATS-6 and AERONET's CIMEL. In addition to this, we think that while a LBL model is used in remote sensing applications its free parameters are tuned to achieve a better agreement with other PWV measurements, in particular, with those, which are considered standard (e.g., MWR). In this way the difference between models in WV continuum strength becomes compensated by other factors. This assertion may be also supported by the report of *Schmid et al.* [2001] that various participants of their study achieved better agreement between their retrievals when each group used its own LBL model than when all of

them used the same version of the LBLRTM code. We think that in order to clarify the WV continuum question, a serious study should be performed comparing different LBL models performance, especially at large PWV column amounts.

3.4. Atmospheric Profiles

[26] Our tests showed that moderate changes in WV, pressure, and temperature profiles used in computations of spectral line broadening have little influence on the retrieval results for SGP CF (differences of the order of 0.001 in a and even less in b, retrieval error of a fraction of per cent). This is true for e.g., replacement of U.S. standard atmosphere profiles by those for mid latitude summer or winter, or even for making calculations assuming sea level site altitude (1013.25 mb pressure) instead of the actual one at SGP CF (318 m, 977 mb pressure). However, for sites with higher altitude (e.g., E1 located at 632 m ASL) or aircraft measurements [e.g., *Livingston et al.*, 2007] correction for altitude will be necessary.

[27] Another way the WV profile and measurement altitude may influence the retrievals is through the effective optical air mass m. This quantity slightly deviates from $(\cos\theta)^{-1}$ (θ is the solar zenith angle) because of refraction of light in the spherical atmosphere and, thus, depends on the profile of atmospheric extinction. This means that optical air masses for aerosols, trace gases, and WV, which profiles are different from that of air, generally differ from the standard "air" air mass [*Kasten and Young*, 1989]

$$m(\gamma) = [\sin\gamma + a \cdot (\gamma + b)^{-c}]^{-1}, \tag{26}$$

where $\gamma = 90^\circ - \theta$ is solar elevation angle (in degrees), and

$$a = 0.50572,\ b = 6.07995^\circ,\ c = 1.6364. \tag{27}$$

The expression for WV air mass was provided in a earlier paper by *Kasten* [1965]. It has the same structure (26), but with different parameters.

$$a = 0.0548,\ b = 2.650^\circ,\ c = 1.452. \tag{28}$$

This paper also included a formula for air m, which appeared to be in error (e.g., $a = 0.15$ in it) and was later corrected by *Kasten and Young* [1989].

[28] As it can be seen from equation (1), in this study we differentiate between air mass types and use the parameters (27) of equation (26) for aerosol and Rayleigh ODs, while the parameters (28) are used for WV. The existing literature on PWV retrievals has examples of both accounting for air mass difference [e.g., *Ingold et al.*, 2000] and neglecting it [e.g., *Michalsky et al.*, 1995]. The difference is indeed small and depends on the actual WV profile during the measurement, which may be different from that (ARDC Model Atmosphere, 1959) assumed by *Kasten* [1965]. For example, *Kiedron et al.* [2001] found that formula (26), (28) overestimates the air masses computed using the instant radiosonde WV profiles in Arctic by up to 3% (but only up to 0.6% for air mass less than 5). Columnar PWV amount is derived from the slant OD in the 940-nm channel after subtraction of aerosol and Rayleigh contributions (with correct air mass factors). Thus air mass in PWV retrieval plays a role only at conversion from slant to vertical column. This means that the erroneous column amount u' computed using air mass m from equations (26), (27) instead of WV air mass m_w from equations (26)–(28) is related to the true amount u as

$$u' = \frac{m_w}{m} u. \tag{29}$$

The factor m_w/m is close to unity at air mass range from 1 to 5 used in our retrievals: m_w exceeds m by less than 0.05% at $m = 1$, reaches 0.5% at $m \approx 3$, 1% at $m \approx 4$, and 1.8% at air mass 5. This means that using the air mass of *Kasten and Young* [1989] instead of that specific for WV leads to a slight overestimation of PWV column amount, especially at large solar zenith angles.

3.5. Instrument Spectral Response Function

[29] The instrument spectral response functions are measured in the laboratory, and the accuracy of these measurements can be evaluated only by repeated tests, preferably using different equipment. Attention should be paid to correct treatment of the measurement noise and offsets, as well as to the SRF's "wings", which should not be chopped off. The instrument's spectral response can also change with time. Inadequate knowledge of the radiometer's SRF affects the data analysis in two ways. First, it leads to a calibration error (since the filter function enters equations (12) and (15)); second, it causes incorrect interpretation of the WV transmittance values since the curve of growth is computed for a wrong SRF (subtraction of aerosol and Rayleigh contribution is also slightly affected). We will describe the effect of erroneous SRF on the PWV retrievals in two situations: when the error has form of a spectral shift, and when the instrument's filter has an out-of-band (OOB) leak allowing light to reach the detector from spectral regions where it is supposed to be blocked.

[30] The calibration effect is easy to estimate analytically using the notations from section 3.1. It follows from equations (12)–(15) that the measured value of the total atmospheric transmittance can be written as

$$T_t^{(f)} = \frac{V}{V_L} \frac{\int f(\lambda) I_L(\lambda) \mathrm{d}\lambda}{\int f(\lambda) I_0(\lambda) \mathrm{d}\lambda}. \tag{30}$$

If f is not accurately known and a nominal SRF f_0 is used instead, we obtain the value

$$T_t^{(f_0)} = T_t^{(f)} \frac{\int f_0 I_L \mathrm{d}\lambda}{\int f I_L \mathrm{d}\lambda} \cdot \frac{\int f I_0 \mathrm{d}\lambda}{\int f_0 I_0 \mathrm{d}\lambda}, \tag{31}$$

which leads to the calibration errors in OD and PWV amount of the forms (18) and (19) with

$$c = \ln\left(\frac{\int f I_L \mathrm{d}\lambda}{\int f_0 I_L \mathrm{d}\lambda}\right) - \ln\left(\frac{\int f I_0 \mathrm{d}\lambda}{\int f_0 I_0 \mathrm{d}\lambda}\right). \tag{32}$$

Note, that if the calibration lamp had the same spectrum as the Sun, c would be equal to zero. We will show below, that the estimated calibration error associated with inadequate

characterization of the instrument's spectral response is smaller than the general calibration accuracy (c up to 0.03) assumed in section 3.1. The effect of a calibration error on the retrievals has been already described in section 3.1, thus, we will not repeat it here.

3.5.1. Spectral Shift

[31] *Michalsky et al.* [2001b] report a 0.8-nm shift in the 940 nm MFRSR filter after a nearly 18-month deployment, resulting in 0.2 cm change in the retrieved PWV (with 3 cm average column). Even larger errors may occur if the actual SRF is not known and either a nominal function or SRF from a different head is used instead. For example, the effective central wavelength of head 922 (Figure 2, top) is 939.6 nm, while head 241C (deployed on E13 MFRSR during the most of 2000) is centered at 938.0 nm, that is, substituting one SRF for another would result in the effect of a 1.6-nm spectral shift.

[32] The calibrational effect of a spectral shift can be estimated from equation (32) if the instrument's SRF is sufficiently narrow to assume that lamp or TOA solar irradiance spectra are constant across the filter transmittance interval. Taking into account that f and f_0 have the same shape and, therefore, the same integrals over wavelength, we can write equation (32) in a simpler form.

$$c = \ln\left(\frac{\tilde{I}_L(\lambda_f)}{\tilde{I}_L(\lambda_0)}\right) - \ln\left(\frac{\tilde{I}_0(\lambda_f)}{\tilde{I}_0(\lambda_0)}\right), \tag{33}$$

where λ_f and λ_0 are central wavelengths of respectively f and f_0, while tilde reflects spectral smoothing of the lamp and solar irradiances due to the integration in (32). Without knowing the spectrum of the lamp used for calibration, we can quantitatively estimate only the second term in equation (33) as being around ±0.005 for a 1 nm shift (the actual value depends on specific filter function and on the direction of the shift). Assuming that the lamp irradiance has spectral variability similar to I_0, we can estimate that c can reach 0.01 by the absolute value, which is 3 times smaller than the general calibration error assumed in section 3.1.

[33] Figure 3 shows the effect on PWV retrievals of a wavelength shift in MFRSR SRF (for head 922) of up to ±2 nm. Figure 3 (top left) compares the original and "shifted" curves of growth. We see that while a positive 2 nm shift is visible only at large (exceeding 20 cm) slant PWV column amounts, a negative shift of the same magnitude plays a more significant role at smaller PWV column range. This behavior is specific for the particular head and is determined by the position of its SRF relative the WV absorption spectrum. Similar behavior is seen in Figure 3 (top right), which shows the dependence on spectral shift of the parameters a and b of the approximate formula (5). We see that the power law exponent b depends on the shift almost linearly, thus, the absolute difference between its "shifted" and original values does not depend on the shift's sign (the original value of b is 0.56, while the negative and positive 2 nm shifts change it respectively to 0.53 and 0.58). The factor a, on the contrary, experiences a notably larger change for negative shifts (from 0.55 to 0.61 for 2 nm shift), than for positive ones (from 0.55 to 0.52). Together with the asymmetric behavior observed in Figure 3 (top left) this indicates, that a change with shift in a, rather than in b, affects the PWV retrievals most. To show the effect of spectral shift on actual retrievals we computed the absolute and relative errors induced by it for typical SGP winter and summer conditions already used above for other tests. The corresponding plots are presented in the Figure 3 (bottom). The computations are made using the actual curves of growth, however, power law approximation using equation (10) with a and b from Figure 3 (top right) yields similar results. We see, that for winter conditions moderate negative and positive 1 nm shifts induce the errors in PWV column amount of respectively −0.025 cm (−5.0%) and 0.015 cm (3.1%), while for summer conditions the corresponding numbers are −0.18 cm (−4.4%) and 0.09 cm (2.3%). As in our other tests, the absolute errors are larger for summer, while the relative errors are larger for winter.

3.5.2. Out-of-Band Transmittance

[34] Along with the main maximum in transmittance described by the manufacturer-supplied nominal SRF, the interference filters used in solar radiometers can have many others. Out-of-band rejection of currently available spectral filters is measured in laboratory using standard lamps. Manufacturers quote the OOB rejection of their filters by a maximal allowed value of transmittance at wavelengths outside the listed spectral interval. This limit is normally between 10^{-7} and 10^{-4}. For example, *Livingston et al.* [2005] report that the data provided by the filter manufacturer for the AATS-14 Sun photometer indicated that blocking in the out-of-band rejection region is between 10^{-7} and 10^{-6} for each filter. BSRN [*WCRP BSRN*, 2001] requires from spectral radiometers that out-of-band rejection should be at least 10^{-4} at wavelengths more than 40 nm away from the nominal filter wavelength. *Schmid et al.* [1998] reported a significant leak of a SPM-2000 Sun photometer 862 nm filter, which constituted 10^{-3} of the filter peak transmission (other filters showed smaller 10^{-4} leaks). *Mavromatakis et al.* [2007] use out-of-band transmittance values ranging from 10^{-6} to 10^{-4} in their sensitivity study dealing with both theoretical (Gaussian) and real (CIMEL, SPM-2000) SRFs. *Villevalde et al.* [1988] estimated that the background transmittance of 10^{-4} may induce an error up to 10% in aerosol optical depth.

[35] The filters most recently installed in the ARM MFRSRs are manufactured by Perkin-Elmer, who claim 10^{-4} OOB rejection limit. Laboratory measurements made in 2001 of OOB rejection for older MFRSR heads [J. Michalsky, private communication, 2008] showed no problems with 870 and 940 nm filters, while some shorter-wavelengths filters had modest leaks (less than 1% of total (integrated over the spectrum) transmittance for 415 nm filters and less than 0.2% for 500 nm filters). This is consistent with the 10^{-4} OOB rejection. We should note, that filter transmission measurements made with e.g., a Cary spectrometer may not have the sensitivity to pick up a small transmission in the spectral region between the long-wave cutoffs of the filter and the detector SRFs (roughly between 960 and 1100 nm), thus, an undetected leak may come from this part of the spectrum. The total SRF of MFRSR spectral channel is a product of diffuser and filter transmittances (the latter with possible OOB leak) and detector quantum efficiency (QE). If the filter leak occurs at the spectral peak of QE its effect on the measurements is enhanced. The detectors installed in MFRSRs have QE

maximum either at 700 nm or 950 nm. In the latter case the enhancement of a leak does not pose a problem for MFRSR's WV channel, since the detector's QE peaks near the filters central wavelength (940 nm). We should also note, that during field deployment a transmission leak may constitute a fraction of the signal, which is different from the laboratory-measured value because of the difference in spectra between the standard lamp and the Sun.

[36] In the case of a spectral leak the actual instrument's SRF can be represented as

$$f(\lambda) = f_0(\lambda) + f_l(\lambda), \tag{34}$$

where f_0 is the nominal SRF which is assumed in the curve of growth computations and is spectrally located mostly within the WV absorption band, and f_l is a small (compared to f_0) leak SRF. The described above measurements of OOB rejection can be used to compute the integrated spectral leak characteristics, which are ratios of the leak transmission to the nominal filter transmission when the instrument is illuminated by TOA solar irradiance

$$\nu_I = \frac{\int f_l I_0 \, \mathrm{d}\lambda}{\int f_0 I_0 \, \mathrm{d}\lambda}, \tag{35}$$

and by a calibration lamp

$$\nu_L = \frac{\int f_l I_L \, \mathrm{d}\lambda}{\int f_0 I_L \, \mathrm{d}\lambda}. \tag{36}$$

These parameters are normally less than 1%.

[37] The calibration error associated with the use of incorrect SRF in the case of transmission leak can be estimated from equation (32) as

$$c = -\ln(1 + \nu_I - \nu_L) \approx \nu_L - \nu_I. \tag{37}$$

Here we used the fact that $\nu_I \ll 1$ and $\nu_L \ll 1$. The value and even sign of c in equation (37) depends on characteristics of a particular leak and calibration lamp, while it does not depend on PWV amount or any other atmospheric characteristics. Assuming that ν_I and ν_L are of the same order of magnitude as

$$\nu = \frac{\int f_l(\lambda) \, \mathrm{d}\lambda}{\int f_0(\lambda) \, \mathrm{d}\lambda}, \tag{38}$$

where integration is performed over a silicon detector sensitivity spectral range (300–1100 nm), we can roughly estimate the value of c as being around 0.01 for 10^{-4} OOB rejection limit.

[38] A larger effect of a OOB leak on the measurements is associated with an increase of transmittance in the 940-nm channel leading to underestimation of the optical depth in this channel and consequently the retrieved PWV content (especially when this content is high). In other words, this means that because of the leak presence the actual curve of growth (4) is lower than the nominal, which is used for PWV retrievals. *Mavromatakis et al.* [2007] comprehensively modeled this effect using realistic atmospheric spectra for sample AERONET and SPM-2000 filter SRFs. They found that for e.g., AERONET's filter function (which is similar to MFRSR's SRF) the 10^{-4} OOB leak (spectrally uniform within the 300–1100 nm detector sensitivity range) results in notable changes of the curve of growth parameters a (from 0.713 to 0.712) and especially b (from 0.587 to 0.575), which indicates that large slant column PWV amounts are affected the most. These changes can be translated using equation (11) into the error in the retrieved columnar PWV for typical SGP conditions: 0.001 cm (0.2%) for winter noon, and 0.12 cm (3%) for summer noon. As expected, these errors are much larger at air mass 5: 0.1 cm (5%) in winter, and 0.25 cm (6%) in summer.

[39] It is not our aim here to perform detailed computations, such as those reported by *Mavromatakis et al.* [2007]. We, however, can derive a simple analytical formula, which will help us to better understand the effect of a leak on PWV retrievals. It will also allow us to estimate the integral parameter ν_I from a pair of curves of growth (with and without transmittance leak), and provide a rough estimate of the OOB transmission value which would be necessary to produce the difference between the theoretical and empirical curves of growth in Figure 2 (bottom). We make two assumptions allowing us to make error estimates without knowing the spectral structure of the leak. First, we neglect the variation of the aerosol and Rayleigh transmittances across the spectrum, and, second, we assume that the leak occurs completely outside WV absorption bands (i.e., $T_w(\lambda) = 1$ where $f_l(\lambda) > 0$). The first condition, while it is not quite justified physically, allows us to use equation (3) for the filter WV transmittance. In reality, presence of a leak means that the instrument's SRF can no longer be considered as narrow, so the transmittances of aerosol and Rayleigh scattering cannot be separated from that of WV. (Equation (3) can be effectively modified if $f_l(\lambda)$ is narrow and its spectral location is known, however this is not normally the case for the diffraction filters.) Using these conditions we can substitute (34) into equation (3) to obtain the actual WV transmittance.

$$T_w^{(f)} = \frac{\int T_w f_0 I_0 \, \mathrm{d}\lambda + \int f_l I_0 \, \mathrm{d}\lambda}{\int f_0 I_0 \, \mathrm{d}\lambda + \int f_l I_0 \, \mathrm{d}\lambda}. \tag{39}$$

Dividing both numerator and denominator by the integral of $f_0 I_0$ (the first term in denominator) and making expansion up to the first order in $\nu_I \ll 1$ (defined by equation (35)) we obtain a simple relation

$$T_w^{(f)} = T_{w0}^{(f)} + \nu_I \left(1 - T_{w0}^{(f)}\right), \tag{40}$$

where $T_{w0}^{(f)}$ is the nominal transmittance of the PWV column amount $u^{(sl)}$ computed according to equation (3) with $f = f_0$. Note, that the structure of the second term in equation (40) (which vanishes when $T_{w0}^{(f)} = 1$) indicates that the measurements of smaller transmittances corresponding to larger PWV amounts are more affected by OOB transmission problem. Equation (40) translates into the following relation between the corresponding optical depths.

$$\tau_w^{(sl)} = \tau_{w0}^{(sl)} - \ln\left[1 + \nu_I \left(\exp\left[\tau_{w0}^{(sl)}\right] - 1\right)\right]. \tag{41}$$

We see from this equation that, since the WV optical depth is always positive, the error associated with a leak always leads to underestimation of $\tau_w^{(sl)}$ and, therefore, columnar PWV retrievals. To use this model we need to "calibrate" it, that is, to relate the parameter ν_I to OOB rejection level. We can do this by estimating ν_I from the described above results of *Mavromatakis et al.* [2007] using equations (40) or (41)

$$\nu_I = \frac{T_w^{(f)} - T_{w0}^{(f)}}{1 - T_{w0}^{(f)}} = \frac{\exp\left(\tau_{w0}^{(sl)} - \tau_w^{(sl)}\right) - 1}{\exp\left(\tau_{w0}^{(sl)}\right) - 1}, \qquad (42)$$

where $\tau_{w0}^{(sl)}$ is their curve of growth for perfect OOB rejection, while $\tau_w^{(sl)}$ corresponds to 10^{-4} OOB rejection limit. Since our model is not perfect, equation (42) gives us ν_I as a function of slant PWV column amount rather than a single value. In the range between 1 and 10 cm (used by AERONET to compute a and b) the median value of ν_I is 0.67%, while between 15 and 25 cm (where the effect of a leak is pronounced the most) it is 0.27%.

[40] Now we can improve the numerical error estimates for typical SGP seasonal conditions using our own head parameters (for head 922) and the above estimate of ν_I = 0.67% in equations (40) or (41) assuming the power law dependence (5). This gives us the new estimates of 0.008 cm (1.6%) for winter noon and 0.09 cm (2.3%) for summer noon, showing the seasonal difference similar to the errors induced by SRF spectral shift, or spectral database change. The difference with the above presented direct estimate using the a and b parameters from *Mavromatakis et al.* [2007] can be explained by the difference in SRFs used. Another possible explanation is that *Mavromatakis et al.* [2007] used the slant PWV column interval from 1 to 10 cm to determine the parameters of their power law approximation, which then may not work perfectly at the interval's end $u_w^{(sl)}$ = 1 cm, which corresponds to our winter noon conditions (in fact, error estimates at air mass 5 show much less seasonal difference).

[41] We used equation (42) to estimate ν_I from the MFRSR and microwave radiometer measurements shown in Figure 2 (bottom), assuming that the transmittance leak is the only source of discrepancy between them. This estimate gave us a factor of 10 larger value ν_I = 2.8% needed to fit the data in the 15–25 cm slant PWV column amount range. Despite that the SRF used by *Mavromatakis et al.* [2007] was slightly different from MFRSR's SRF used for the latter estimate, we can assume that for the same OOB rejection limit the values of ν_I computed for these two filter functions should be similar. Thus taking into account that ν_I is linear with respect to f_l, we can conclude that to explain the MFRSR–MWR discrepancy we should assume OOB transmission of 10^{-3}. While such a strong leak is technically possible, we do not believe that it can be characteristic for all MFRSRs and other solar radiometers (AERONET's CIMEL and particularly the well-characterized AATS-6), all of which (as we will describe below) have shown measurements systematically smaller than those from MWRs in the large PWV value range. Thus we conclude, that an exceptionally large OOB leak in the MFRSR filter transmittance cannot be a realistic explanation for the disagreement with microwave radiometer measurements.

Table 1. Estimated Uncertainties in MFRSR-Derived Retrievals of PWV Column Amount Associated With Various Sources[a]

	Winter	Summer
Calibration	0.05 cm (10%)	0.18 cm (4.5%)
Correction for AOD	0.03 cm (6%)	0.06 cm (1.5%)
Spectral databases	0.025 cm (5%)	0.20 cm (5%)
Head's SRF shift	0.025 cm (5%)	0.18 cm (4.4%)
OOB transmission	0.008 cm (1.6%)	0.09 cm (2.3%)

[a]The estimates are made for solar noon and typical winter and summer atmospheric conditions at SGP site using SRF for MFRSR head 922.

3.6. Summary of Uncertainties

[42] We showed that PWV retrievals from MFRSR data may be influenced by a range of uncertainties of different nature. The magnitudes of these uncertainties for atmospheric conditions typical for the SGP site (0.5-cm PWV column, air mass 2 (at noon) in winter; and 4-cm PWV column, and air mass at noon 1.03 in summer) are summarized in Table 1. These estimates show that a 3% calibration error for the 940-nm channel translates into an error in retrieved PWV column amount of 0.05 cm (10%) in winter and 0.18 cm (4.5%) in summer. Correction for Rayleigh scattering OD may introduce only negligible error, while subtraction of AOD from 940-nm channel optical depth may affect PWV retrievals by 0.03 cm (6%) in winter and 0.06 cm (1.5%) in summer (these values are obtained assuming typical seasonal aerosol load at SGP). The error due to incorrect WV absorption data in spectral databases is difficult to quantify, since these databases continue to be updated. We estimate, that the errors in HITRAN 1996 database result in 15% overestimation in PWV column amount compared to the latest HITRAN 2004, which, we hope, is much closer to reality. On the other hand, we see a 5% underestimation of retrieved PWV column if the ESA-WVR database is used instead of HITRAN 2004. PWV retrieval errors may also be induced by a spectral shift in the MFRSR head SRF resulting either from filter degradation, poor laboratory characterization, or using an SRF from a different instrument's head. Our estimates for head 922 showed differences depending on the sign of the shift, with negative shifts inducing larger PWV errors (underestimation by 0.025 cm (5.0%) in winter, and by 0.18 cm (4.4%) in summer for a 1 nm shift). The errors due to OOB transmittance estimated based on the results of *Mavromatakis et al.* [2007] assuming the typical for MFRSR OOB rejection limit of 10^{-4} are 0.008 cm (1.6%) for winter noon and 0.09 cm (2.3%) for summer noon. In theory, some error in PWV retrievals by MFRSR may occur at large solar zenith angles because of the angular dependence of instrument's filters spectral responsivity coupled with imperfect performance of the diffusor, which allows change in the angle of incidence of light on the filter surface during the day. However, comparison with normal incidence Sun photometers (CIMEL, AATS-6) shown in Figures 4 and 9 do not show specific deviations in retrieved PWV column amount from MFRSRs at low Sun angles (at least for air masses smaller than 5 used for retrievals), thus, we consider this effect to be negligible.

[43] The above described tests lead us to conclude, that uncertainties in calibration and in the instrument's spectral response are the two largest instrumental sources of error in

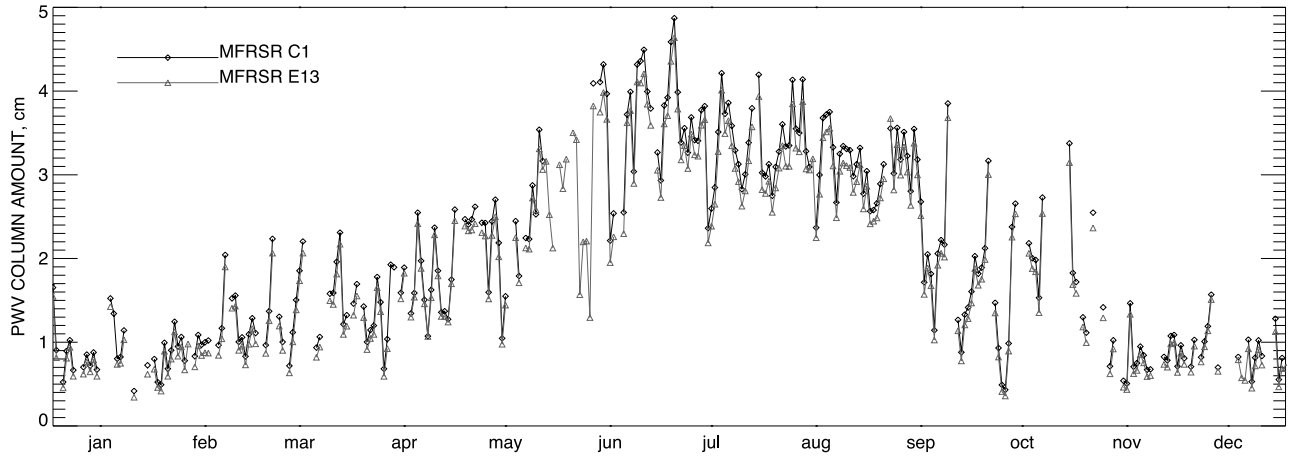

Figure 4. Retrievals of column PWV for the year 2000 data from the two MFRSRs at SGPs Central Facility (C1 and E13).

PWV retrievals, each of which may induce an error of up to 0.2 cm. In addition to these errors, there is a comparable in magnitude uncertainty induced by disagreement between current WV spectral absorption databases (HITRAN 2004 and ESA-WVR). Simply adding these error estimates would give us a low retrieval accuracy. However, in reality, some of these errors may be smaller and/or cancel each other. To asses the real measurement accuracy (specific to a particular instrument) we made a number of intercomparisons with other measurements of similar and different types. Besides the accuracy estimate, these intercomparisons may help to evaluate the effectiveness of tuning MFRSR retrievals by e.g., collocated MWR measurements. This approach [*Schmid et al.*, 2001] implies using the empirical curve of growth (like the one in Figure 2, bottom) instead of those computed according to equation (4). Note, that, provided high accuracy of MWR measurements, this technique corrects all retrieval errors described above, except for the smallest among them associated with AOD subtraction.

4. Results and Intercomparisons

[44] To evaluate the performance of the presented PWV retrieval method, we compare our retrievals from the two SGP Central Facility (36.61° N, 97.49° W, 318 m ASL) MFRSRs (C1, E13) with results of other measurements. For the measurements routinely available at SGP's CF (such as MWR, GPS and AERONET's CIMEL) we present comparisons based on a 1-year-long data set from 2000, while we make more validation tests using the data from the water vapor intensive observation period (WVIOP2000, September–October 2000), when additional instrumentation was deployed at the site. We should note, that in this study we are interested only in validation of MFRSR PWV retrievals and will not address disagreements between other instruments.

4.1. One-Year Data Set From 2000

[45] We performed retrievals of PWV column amounts for the data from all SGP Extended Facilities for the year 2000. However, at the time of data processing we did not have complete instrument head data for some sites (this is now being improved, since in the newly reprocessed ARM MFRSR product head characteristics, including SRFs, are being embedded in each data file). Thus, in this study we focus on the Central Facility MFRSRs (C1, E13), for which the technical information was available, while using retrievals from other SGP's EFs in a qualitative manner. Figure 4 shows the PWV retrievals (daily means) from C1 and E13 MFRSRs for the year 2000. A strong summer maximum in PWV column amount is clearly seen. Some data examples are also shown in Figure 9. These MFRSR retrievals were compared with correlative PWV measurements by other instruments routinely available at SGP's CF, which include microwave radiometer (C1 MWR), a Global Positional System (GPS) receiver at the NPN site LMNO2 (Lamont, Oklahoma), and AERONET's CIMEL Sun/sky radiometer (''Cart_Site'' location).

[46] The CIMEL Sun/sky radiometer operated at SGP's CF by AERONET [cf. *Holben et al.*, 1998] points to the Sun based on an ephemeris calculation and then fine tunes the pointing with an active Sun-sensor adjustment. Samples consist of triplets of measurements repeated at every 0.25 air mass for air masses between 2 and 7 and every 15 min for air masses less than 2. The instrument's field of view is 1.2°. The instrument's calibration is transferred from the master instrument calibrated at Mauna Loa site using Langley analysis. Two CIMEL instruments were deployed consequently at SGP's CF during the year 2000: CIMEL 99 (until 28 September) and CIMEL 98 (from 4 October). In this study we use the most recent Version 2 Level 2 AERONET data, which have been cloud screened and quality assured according to *Smirnov et al.* [2000]. The PWV retrieval technique [*Smirnov et al.*, 2004] used by AERONET is similar to ours: it is based on equation (5) with parameters a and b derived by fitting the curve of growth (computed using the HITRAN 2000 spectral database) for slant PVW column amounts between 0 and 10. The SHARM radiation code [*Lyapustin*, 2005] is used to account for the standard atmospheric profiles. We see in Figure 5 (left) good agreement of the retrievals from C1 (−3% bias and −0.07 cm offset) and especially E13 (2% bias and −0.02 cm offset) MFRSRs with the AERONET data set from the year 2000. We will see below that this agreement is substantially better than that between

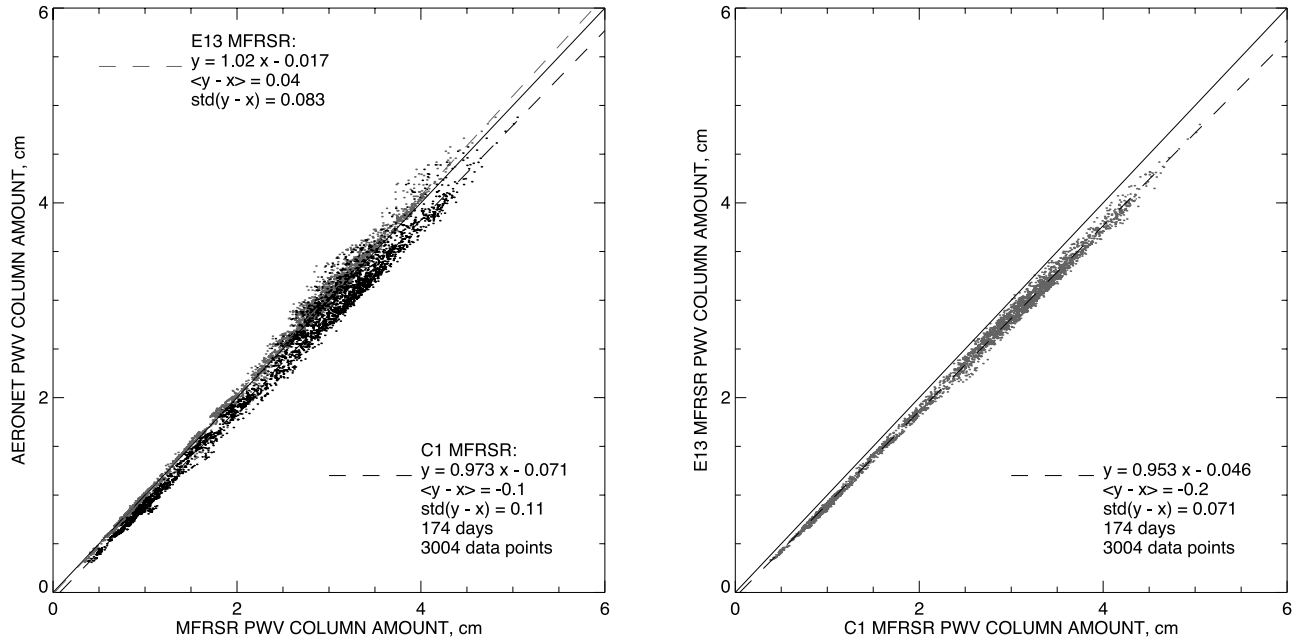

Figure 5. (left) Comparison between column PWV retrievals from C1 and E13 MFRSRs and those from collocated AERONET's CIMEL Sun photometer (''Cart_Site''). (right) The difference in retrievals between the two MFRSRs (sampled at AERONET's measurement times) is probably due to calibration errors (especially in E13 data set).

MFRSR and MWR retrievals. We will also see that retrievals from another solar radiometer (AATS-6) are also closer to those from MFRSRs and AERONET than to MWR measurements.

[47] Figure 5 (especially the right) clearly shows a systematic 5% difference between the PWV values from collocated C1 and E13 MFRSRs. This may be due in part to uncertainties in the laboratory-measured spectral responses of their 940 nm filters. However, our tests show that calibration differences are likely to play a more important role in this disagreement. These tests were described in section 3.1 and are based on equation (21), where we use C1 MFRSR PWV retrievals as the standard measurement (instead of MWR in equation (21)). It appears that the calibration bias can explain the retrieval error in the E13 data set relative to this standard measurement. Figure 6 shows calibration bias time series computed according to equation (21) as described above. The top plot shows daily mean calibration biases for the year 2000 with E13 MFRSR head changes clearly indicated. While head 922 remained on C1 MFRSR for the whole year, E13 MFRSR's head 241C was replaced by head 905C between 10 April and 23 May. Figures 6 (middle left and right) plots corresponding respectively to 2 January and 6 September show that the calculated calibration bias is constant during the day and has the same value. The stability of the calibration bias, as long as head 241C is on E13 instrument, is also seen in the top plot with median values close to -0.045 both before and after the head replacement. These observations suggest that the difference in PWV measurements between the two MFRSRs is mostly caused by the difference in their calibration. The situation is quite different during the period when head 905C was installed on E13 instrument. This is not only because in Figure 6 (top) the mean calibration biases during this period notably differ from the rest of the year (which is not surprising, since one of the heads is different), but rather because these biases are no longer constant during the day, as it is shown in Figure 6 (bottom left). This indicates strong presence of factors other than calibration affecting PWV measurements made with head 905C, most likely inadequate head's spectral response characterization. Figure 6 (bottom right) shows that the calibration bias of E13 MFRSR relative to MWR measurements computed according to equation (21) also has a strong diurnal variation. This means that agreement between MFRSR-derived PWV column amounts and MWR measurements cannot be achieved simply by adjustment of MFRSR calibration. In the above, we came to the same conclusion analyzing the curves of growth in Figure 2 (bottom).

[48] The C1 MWR used in this study is a commercially available ground-based microwave radiometer (cf. the vendors Web site www.radiometrics.com) that senses downwelling radiant energy at 23.8 and 31.4 GHz. Water vapor emission dominates the signal in the 23.8 GHz channel, which is on the wing of the 22.2 GHz water vapor absorption line. Measurements are made every 20 sec. Currently the ARM Program provides 3 different PWV retrieval products derived from MWR measurements. One of them is the original ARM product available from the main ARM Data Archive as 1 or 5 min averages, while the two other (*stat2* and *phys*) are obtained utilizing the recent MWR RETrieval (MWRRET) algorithm [*Turner et al.*, 2007] and are parts of D. Turner's ARM PI data set. The MWRRET algorithm incorporates output from two advanced retrieval techniques, namely, a physical-iterative approach and a computationally efficient statistical method. The forward model used in both methods is the monochromatic radiative transfer model MonoRTM [*Clough et al.*,

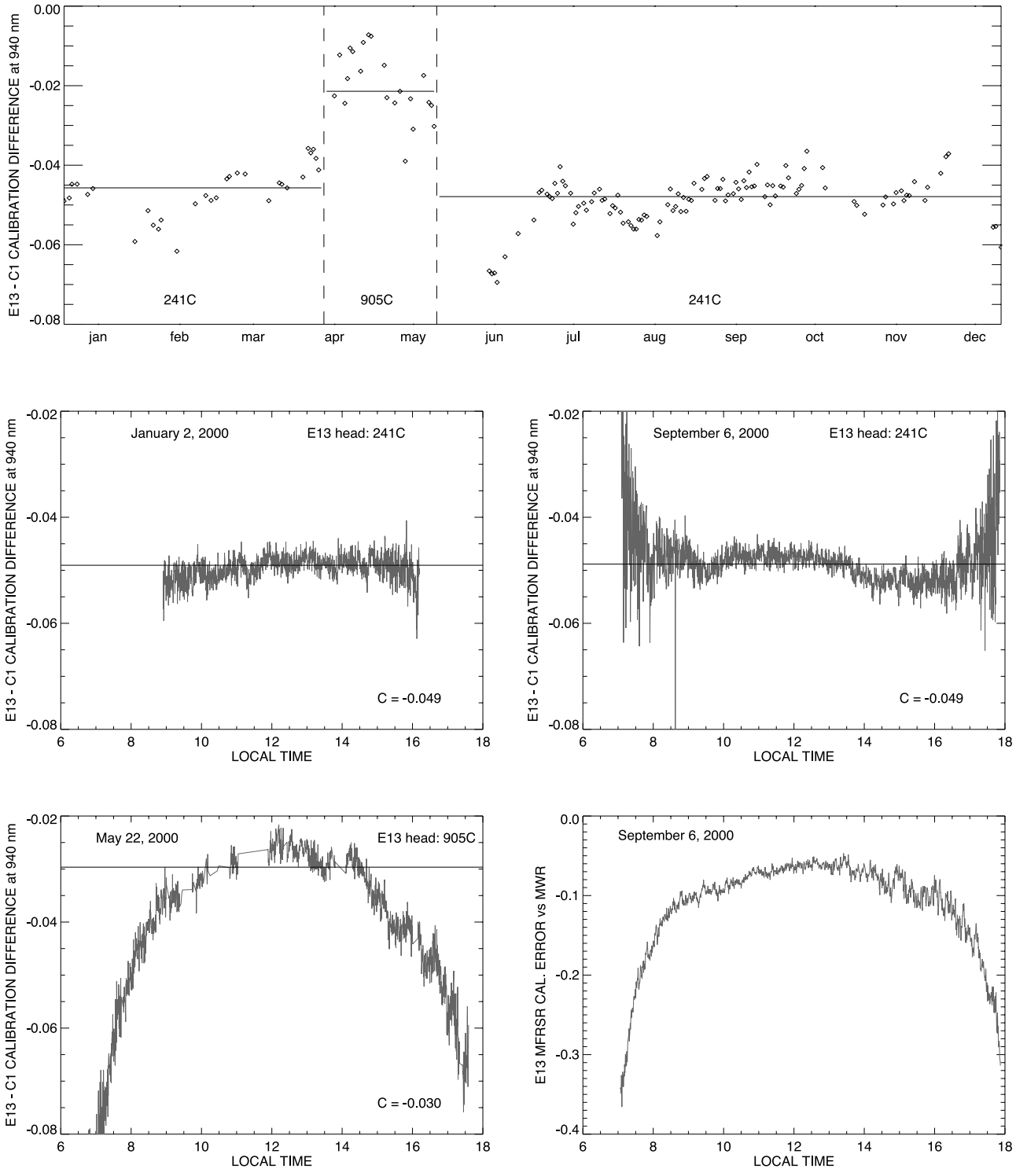

Figure 6. Estimates of possible calibration error from difference in retrieved PWV column amounts. (top) Time series for the year 2000 of daily median calibration error of E13 MFRSR compared to C1 instrument, which PWV measurements are taken as the standard. The dashed lines separate intervals when different heads were installed on the E13 instrument (head 241C was replaced by head 905C from 10 April to 23 May). C1 head 922 remained unchanged throughout the year. Solid lines show intervals' median calibration differences. (middle) Daily time series for 2 January and 6 September (head 241C on E13 MFRSR). (bottom left) Daily time series for 22 May (head 905C on E13 MFRSR). (bottom right) E13 MFRSR calibration error estimate for 6 September made using MWR PWV measurements as the standard.

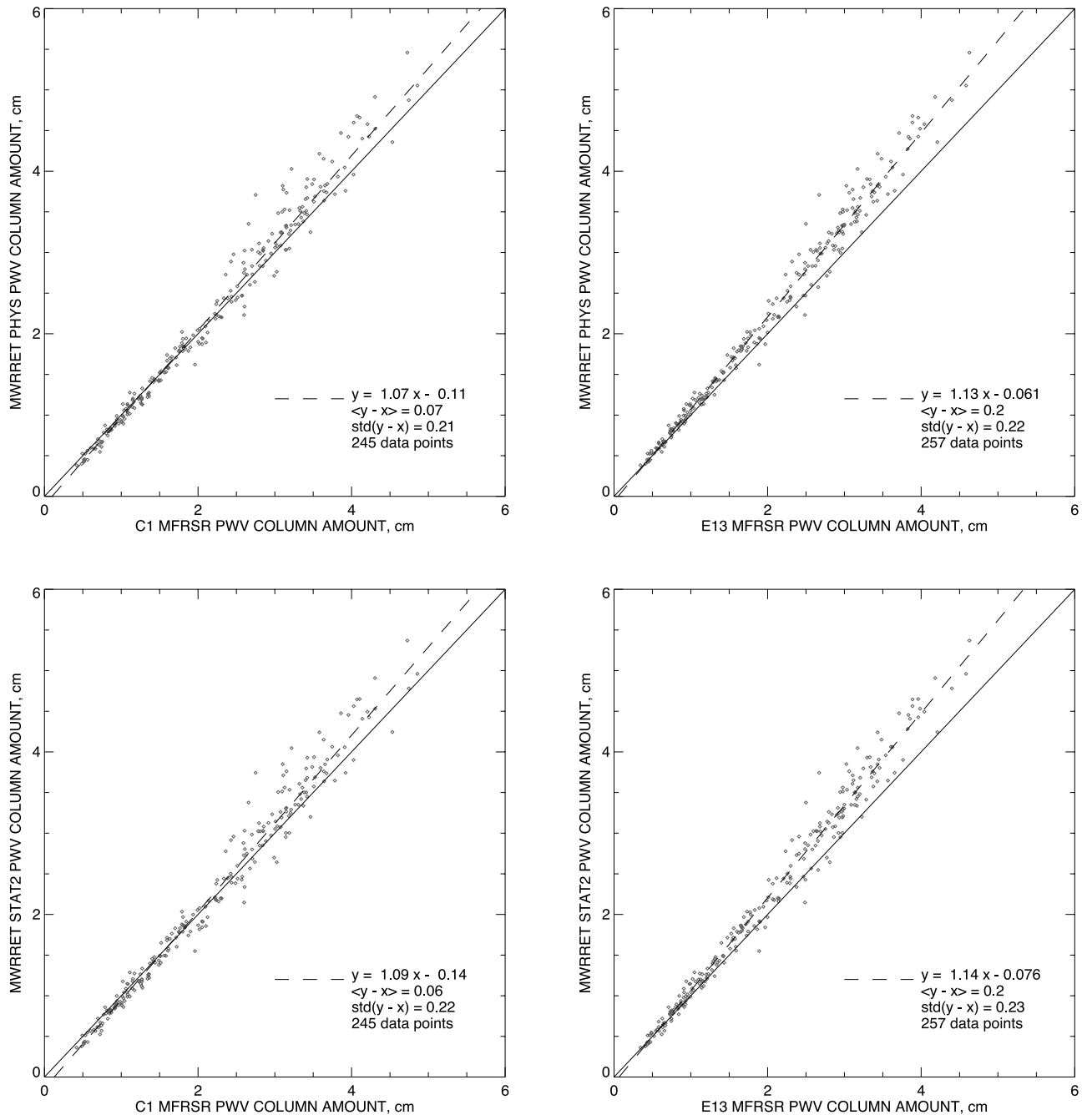

Figure 7. Comparison of column PWV retrievals from (left) C1 and (right) E13 MFRSRs with MWRRET (top) *phys* and (bottom) *stat2* retrievals from C1 MWR. All comparisons are made at *phys* data points in the whole year of 2000.

2005]. The ARM program has used a statistical retrieval method [*Liljegren and Lesht*, 1996] to derive the original PWV product. For inverting the observed microwave brightness temperatures this method utilizes monthly coefficients obtained by averaging over a large historical database of radiosonde profiles for a wide range of atmospheric conditions. This approach is very fast computationally but the retrieved PWV may have errors if the current conditions are different from the assumed monthly means. The more accurate *stat2* product utilizes a statistically derived relationship between the instantaneous retrieval coefficients and surface-based meteorological conditions [*Liljegren et al.*, 2001]. Finally, the most accurate *phys* product is based on the atmospheric temperature profiles and water vapor distribution estimates from collocated/coincident radiosonde data. This physical-iterative retrieval method is more computationally expensive than the *stat2* approach because the forward model is run for each observation. Its advantage in accuracy is also limited to the immediate proximity of the radiosonde launch, thus *phys* data set is rather sparse providing only few measurements a day. We consider *phys* product as the best standard for intercomparisons, however, *stat2* product will be also used in some cases. In fact, for the C1 MWR data set from year 2000 (daytime measurements)

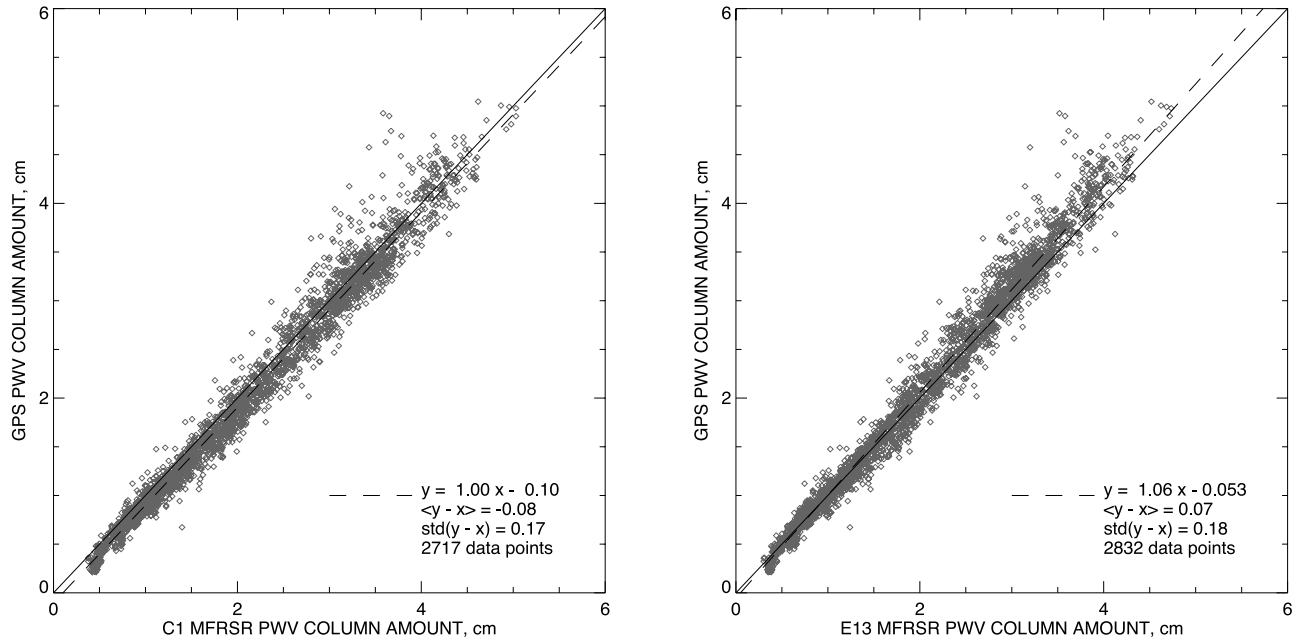

Figure 8. Comparison between PWV retrievals from (left) C1 and (right) E13 MFRSRs and correlative measurements by NPN GPS receiver for the whole year of 2000.

phys and *stat2* data sets are very close to each other: *stat2* retrievals are practically unbiased compared to the *phys* data set, while the standard deviation of the differences between them is only 0.04 cm. The original ARM product for the same period, being also unbiased relative to MWRRET *phys* data set shows larger (0.11 cm) standard deviation of the differences with it (which may be due, however, to presence of a few outlier data points in the original data set). The PWV column amounts retrieved from the 22 GHz spectral line have demonstrated [*Revercomb et al.*, 2003; *Turner et al.*, 2007] consistency with Raman lidar calibrated using a chilled mirror hygrometer in situ measurements – another fundamental PWV retrieval technique.

[49] The comparison between MFRSR PWV retrievals and any of the MWR products shows substantial systematic difference taking form of both biases and offsets. Figure 7 (left) shows that both *phys* and *stat2* PWV column amounts have large positive biases (respectively 7 and 9%) and negative offsets (respectively −0.11 and −0.14 cm) relative the values derived from C1 MFRSR data. The relative biases between E13 MFRSR and MWR retrievals (Figure 7, right) are even larger (13% and 14%), while the offsets are smaller (respectively −0.06 and −0.08). While the geometries of MFRSR and MWR measurements are different (MFRSR "looks" at the Sun, while MWR is pointed to zenith), this seems unlikely to cause such large systematic differences during the whole day.

[50] The GPS receiver at the NPN site LMNO2 is located at 36.69° N, 97.48° W, 9.5 km (5.9 mi) north from the SGP's CF, and about 12 m lower (306 m ASL). This distance may cause some random measurement differences with the CF instrumentation, however is unlikely to result in systematic biases. The PWV column amount retrievals with 30 min resolution from this station are available from the ARM Archive or from the NOAA GPS-Met web site at http://gpsmet_test.fsl.noaa.gov/. There are three major software packages currently in use for estimating the tropospheric signal delay: GYPSY developed at the NASA Jet Propulsion Laboratory (JPL); GAMIT developed at the Massachusetts Institute of Technology (MIT), and Bernese developed at the University of Bern. NPN uses GAMIT, while SuomiNet, another GPS Network operating at the SGP site since 2001, uses Bernese. While PWV retrievals from MWR measurements are relatively straightforward [*Westwater*, 1993], the retrieval of PWV from GPS tropospheric signal delays involves certain assumptions about the lower atmosphere and an estimation process that models the GPS signal delay caused by the refractivity of the neutral atmosphere as a nuisance parameter [*Mikhail*, 1976] in the calculation of GPS antenna position. In general, different geodetic processing software packages employ somewhat different strategies to do this, all with the goal of estimating the 3-dimensional position of the GPS antenna in time with the highest possible accuracy and precision. However, when a common protocol is used in the estimation process [*Fang et al.*, 1998], all software packages achieve similar accuracy for antenna position, and water vapor retrieved from tropospheric signal delay estimates are now in reasonably good agreement (better than 5% in summer) around the world as discussed by *Smith et al.* [2007]. The NPN retrievals available from the ARM Archive show a 7.5% underestimation bias during 2000 relative to MWRRET *stat2* data set (comparison with *phys* data was not possible because of the low temporal resolution of both data sets resulting in virtual absence of simultaneous measurements). This bias leads to a better agreement (Figure 8) of MFRSRs with GPS (no bias and −0.1 offset for C1, 6% bias and −0.05 cm offset for E13) than with MWR.

4.2. Water Vapor IOP 2000

[51] A water vapor intensive observation period (WVIOP2000) was conducted at the SGP Central Facility

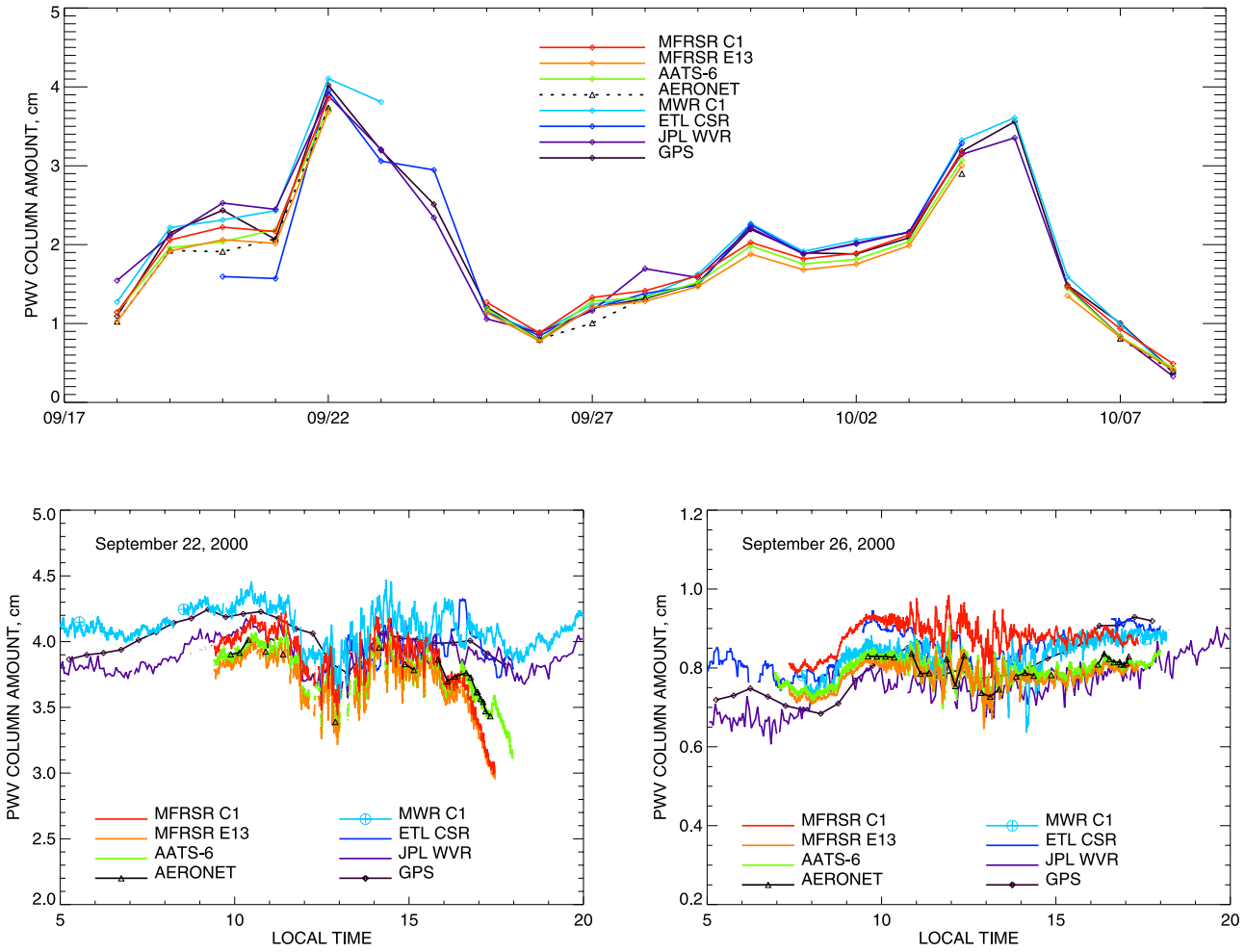

Figure 9. Retrievals of column PWV from WVIOP2000. The presented measurements were made at SGP's Central Facility from 18 September to 8 October 2000 by 4 solar radiometers (C1 and E13 MFRSRs, AATS-6, and AERONET's CIMEL), 3 microwave radiometers (C1 MWR, ETL CSR, and JPL WVR), and NPN GPS receiver. (top) Time series of daily mean PWV column values during the IOP. (bottom) Examples of daily PWV time series for days with high (22 September) and low (26 September) PWV content. MWRRET *stat2* product is used for C1 MWR time series, whereas *phys* retrievals are shown by large crossed circles.

from 18 September to 8 October 2000 [*Revercomb et al.*, 2003; *Cimini et al.*, 2003]. The goal of this effort was to better characterize and improve the accuracy of several PWV measurements, such as MWR, GPS, Raman lidar, radiosondes, etc. While some of these measurements are available at SGP's CF on routine basis, additional instrumentation was brought in for the IOP, including two microwave radiometers: the NASA Jet Propulsion Laboratory (JPL) three-channel water vapor radiometer (WVR) and the NOAA Environmental Technology Laboratory (ETL) dual channel Circulary Scanning Radiometer (CSR). The NASA Ames Research Center six-channel Airborne Tracking Sun photometer (AATS-6) was deployed on the ground during the IOP. The IOP period was characterized by sufficient duration of cloud-free conditions and a wide variation range of observed PWV amounts. Figure 9 (top) presents time series of daily mean PWV column amount retrievals during the IOP by 8 instruments: 4 solar (C1 and E13 MFRSRs, AATS-6, and AERONET's CIMEL) and 4 nonsolar (C1 MWR, ETL CSR, JPL WVR, and NPN GPS receiver). Figure 9 (bottom) plots show daily time series of the retrievals for a day with high PWV content (22 September, Figure 9 (left)) and a day with low PWV content (26 September, Figure 9 (right)). E13 MFRSR retrievals during the IOP show (in point by point comparison) 3.3% underestimation bias and −0.08 cm offset compared to C1 MFRSR data.

[52] The AATS-6 (see *Matsumoto et al.* [1987] and *Schmid et al.* [2001] for technical characteristics) uses an active Sun sensor to keep the instrument pointed at the solar disk. The field of view of the instrument is 3.7°. A measurement sequence consists of an average of nine scans over all six channels taken within 3 sec. This sequence is repeated at 12-sec intervals. The PWV retrievals from AATS-6 data were based on equation (5) with coefficients a and b computed using the HITRAN 2000 spectral database (retrievals with the ESA-WVR database are also available).

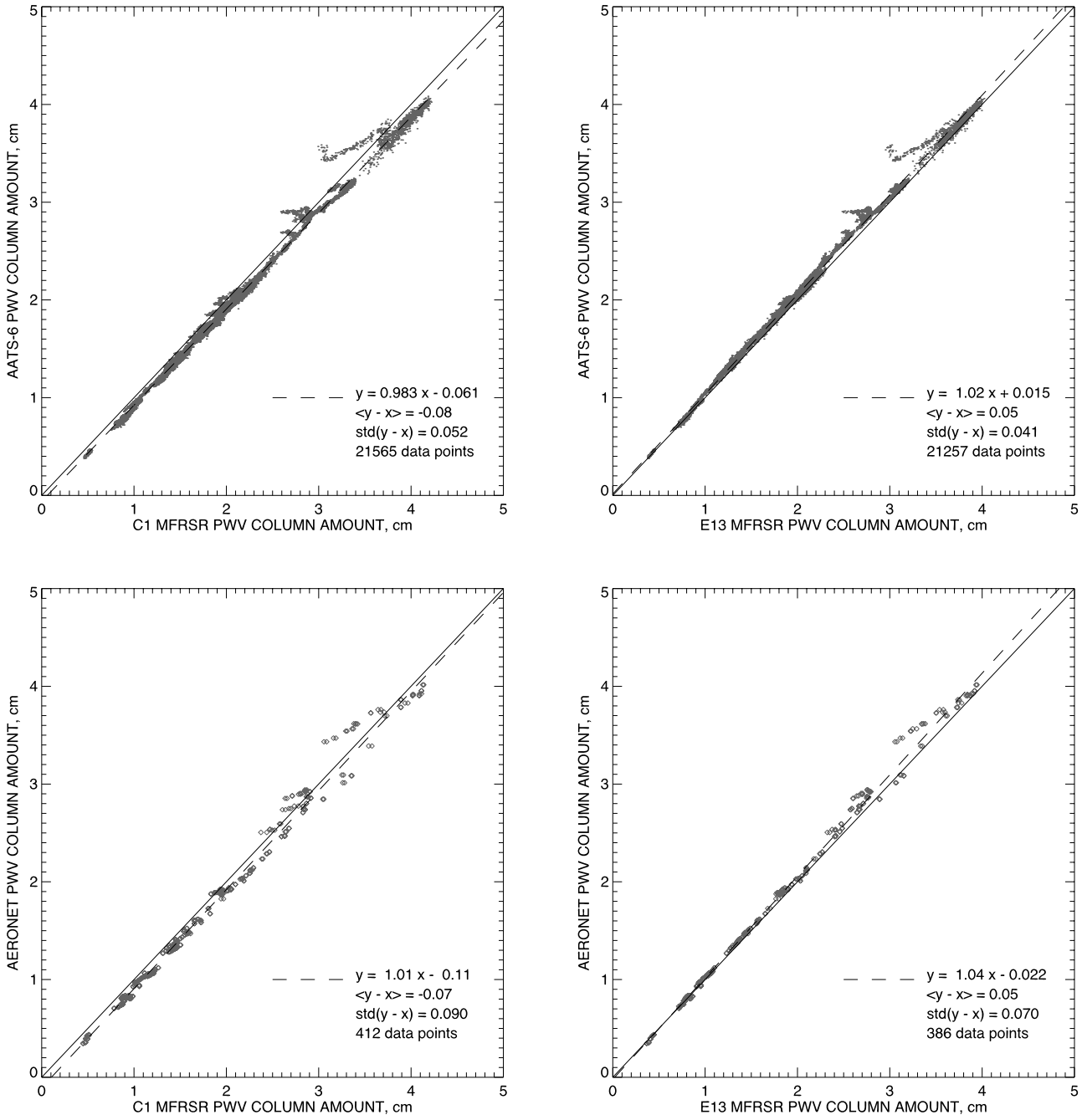

Figure 10. Comparison between (left) C1 and (right) E13 MFRSR PWV retrievals during WVIOP2000 and other PWV measurements using solar techniques ([top] AATS-6 and [bottom] AERONET).

[53] Figure 10 shows intercomparisons between PWV retrievals from the MFRSRs and from other solar instruments (AATS-6, AERONET's CIMEL). We see from the top plots that AATS-6 is in good agreement with both MFRSRs having its values in between those from C1 (−2.7% bias, −0.06 cm offset) and E13 (2% bias, 0.015 cm offset) instruments. Note, that the AATS-6 retrievals made using the ESA-WVR database produce values 8% lower than these in Figure 10 (top). These values are lower by 5.2% than E13 and by 9.5% than C1 MFRSR retrievals. As we pointed out above, using the more recent HITRAN 2000 or 2004 spectral database in MFRSR data analysis also results in 5% increase in PWV column amount relative to ESA-WVR-based retrievals. As it can be seen in Figure 9, AERONET's measurements during the IOP, unfortunately, were quite sparse because of replacement of the CIMEL instrument (no data taken from 28 September to 4 October). The smaller number of data points increases the random error in the regressions (Figure 10, bottom) resulting in e.g., positive 1% observed bias between AERONET and the C1 MFRSR retrievals (offset is −0.11 cm), while in the full-year intercomparisons (Figure 5, left) this bias is negative.

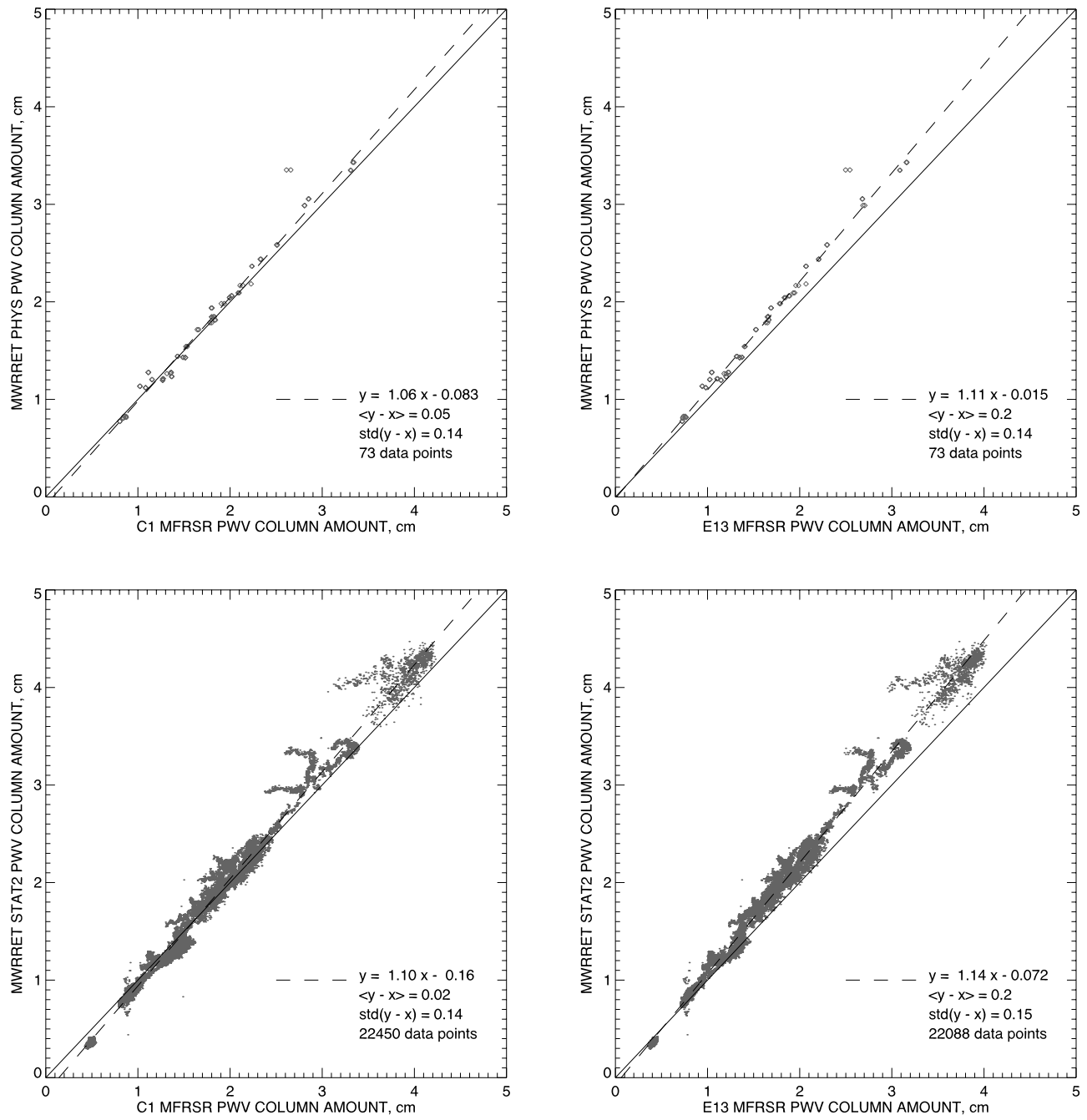

Figure 11. Comparison of columnar PWV retrievals from (left) C1 and (right) E13 MFRSRs made during WVIOP2000 with correlative C1 MWR data (MWRRET [top] *phys* and [bottom] *stat2* data sets).

AERONET's retrievals have 4% bias and −0.02 cm offset relative the E13 MFRSR, and, as in AATS-6 case the most of AERONET data are in between the C1 and E13 MFRSR values.

[54] Point by point comparisons of MFRSR retrievals with MWRRET *phys* and *stat2* data products are shown in Figure 11. The observed differences are similar to those in 1-year data sets Figure 7. C1 MFRSR shows 6% bias and −0.08 cm offset compared to *phys* data, and 10% bias and −0.16 offset relative *stat2*. The corresponding E13 MFRSR numbers are 11% bias and −0.015 cm offset for *phys* and 14% bias and −0.07 offset for *stat2*. Note, that the regressions for *phys* and *stat2* data sets and the same MFRSR in Figure 11 show larger differences than in Figure 7 because here *stat2* is not sampled at the *phys* data points.

[55] The ETL CSR microwave radiometer makes measurements at 20.6 and 31.64 GHz with resolution 1–2 min. The JPL WVR has 3 spectral channels (20.7, 22.2, and 31.4 GHz), one of which (22.2 GHz) coincides with the center of the WV absorption line. Measurements are made every 3–4 min. The instruments were calibrated using tipping curve algorithms [*Han and Westwater*, 2000]. These instruments and their calibration procedures are described in detail by *Cimini et al.* [2003]. PWV retrievals from ETL CSR

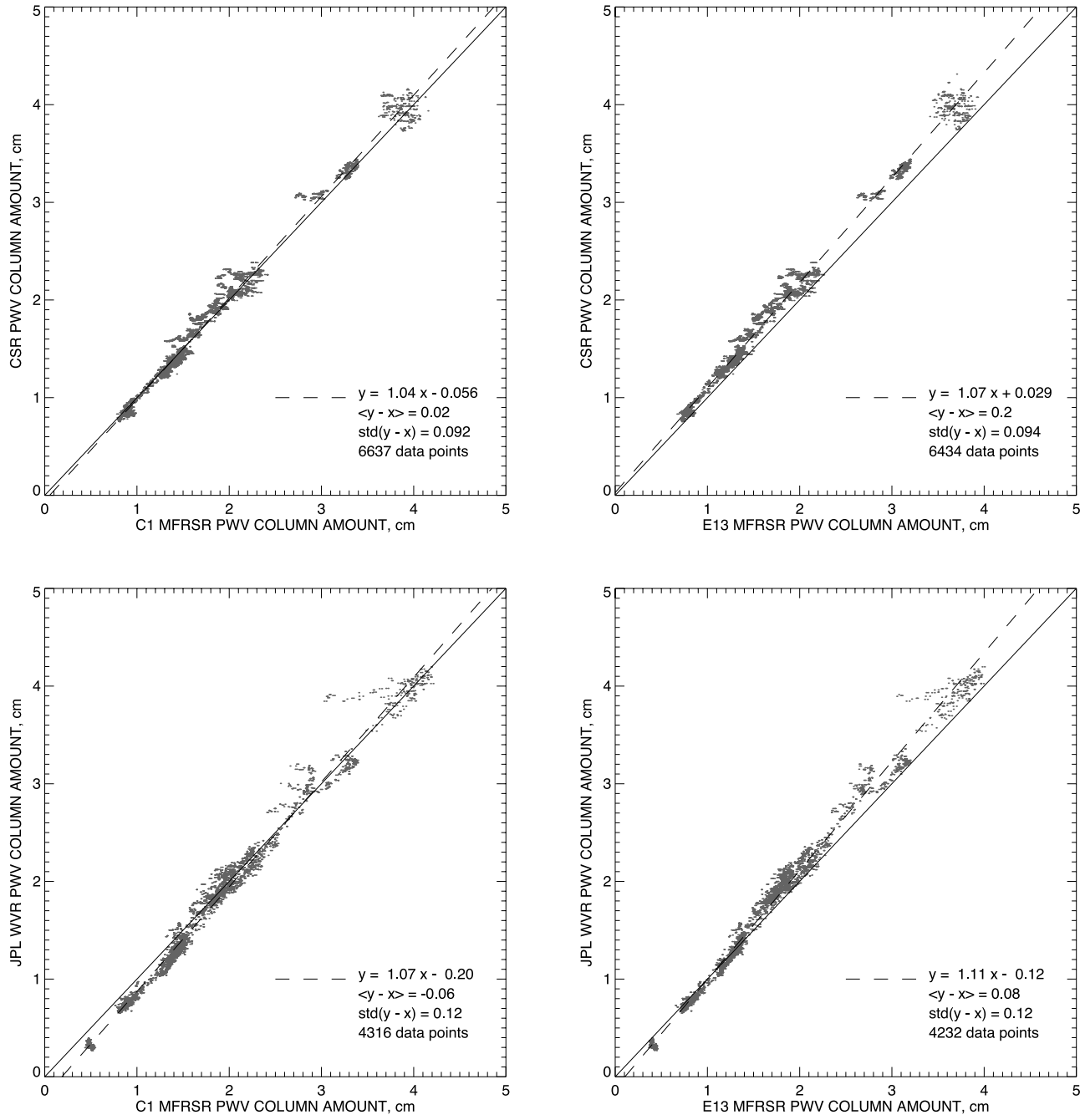

Figure 12. Comparison of columnar PWV retrievals from (left) C1 and (right) E13 MFRSRs made during WVIOP2000 with correlative measurements by (top) ETL CSR and (bottom) JPL WVR microwave radiometers.

and JPL WVR measurements during the IOP are in good agreement with MWRRET *phys* data set derived from C1 MWR data: CSR-derived values exceed *phys* values only by 2%, while JPL WVR retrievals are 2.8% lower than *phys* with −0.055 cm negative offset. However, because of the small number (30–40) of *phys* data points coinciding with CSR and/or WVR measurements during the IOP these bias estimates may be affected by random error. Comparisons of CSR and JPL WVR retrievals with those from C1 MFRSR are shown in Figure 12. As may be expected from the good agreement of the guest microwave radiometers with the C1 MWR, both comparisons show similar to MWR (and even slightly better) agreement with MFRSR data. The ETL CSR shows 4% bias and −0.06 cm offset relative the C1 MFRSR, and 7% bias and 0.03 cm offset relative the E13 instrument. JPL WVR shows 7% bias and −0.20 cm offset compared the C1 MFRSR, and 11% bias and −0.12 cm offset relative the E13 MFRSR.

[56] NPN GPS PWV retrievals in the long-term data set from the main ARM Archive are slightly smaller (0.075 cm offset) than in the data from the IOP section. This difference was caused by an error in the algorithm used to estimate the

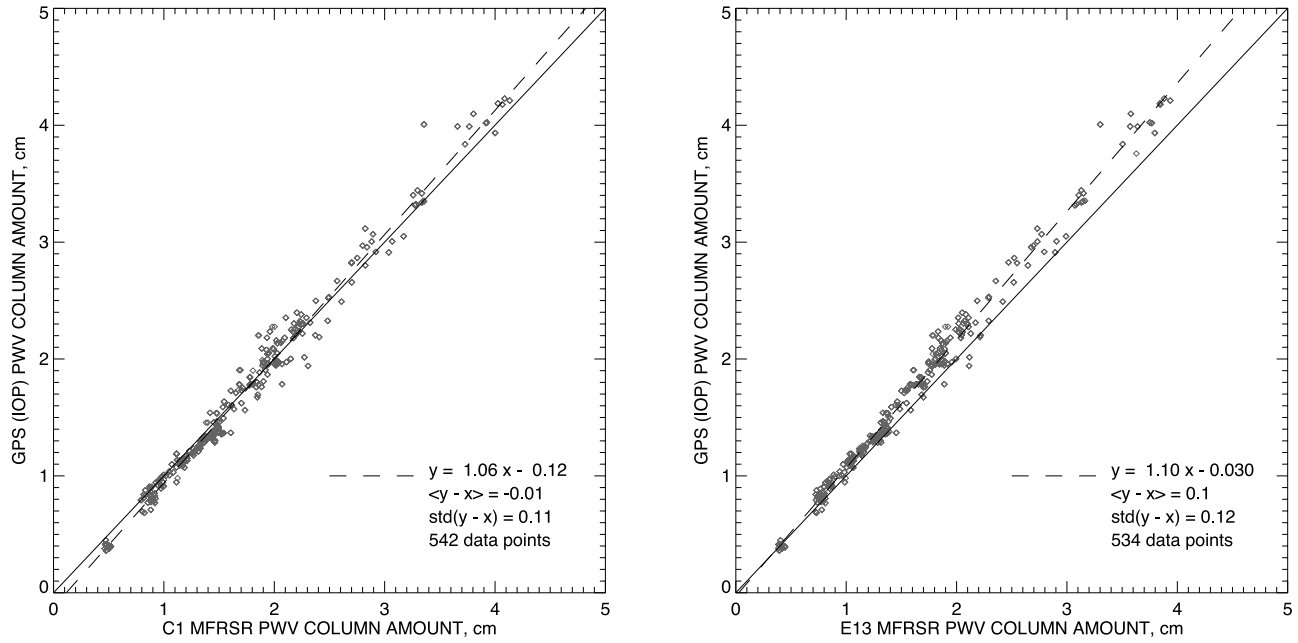

Figure 13. Comparison between PWV retrievals from (left) C1 and (right) E13 and correlative measurements by NPN GPS receiver for WVIOP2000 (GPS values are from the IOP Archive).

zenith hydrostatic (dry) signal delay (ZHD) from station surface pressure, latitude and elevation. The error, which was detected after the IOP ended, was overestimating the ZHD by about 0.5 cm which equates to a dry bias of about 3/4 mm in PWV. The error was corrected and incorporated into the IOP data archive but (apparently) not into the main ARM archive. This correction generally improves GPS agreement with MWR, however, being an offset adjustment, it does not change the relative bias between these two instruments (as well as that between GPS and the MFRSRs). The MWR-GPS bias appeared to be smaller during the IOP than for the whole year (4.5% versus 7.5%). Thus comparison of GPS retrievals with MFRSR during the IOP (Figure 13) shows larger overestimation biases (6% for C1 and 10% for E13) relative to 0% and 6% biases (respectively for C1 and E13 MFRSR) in the comparison for the whole year (Figure 8). The offsets in Figure 13 are -0.12 cm for C1 and -0.03 cm for E13 MFRSR. If the above mentioned correction was applied to the whole GPS data set, the mean difference ($\langle y - x \rangle$) in Figure 8 would change from -0.08 to -0.155 cm for the C1 MFRSR and from 0.07 to -0.005 cm for the E13 instrument. The offsets would change accordingly, while the relative biases and the standard deviations of the differences should remain intact.

4.3. Spatial Variability of Water Vapor Column Amount

[57] The high spatial density of the SGP MFRSR network allows us to reliably interpolate between PWV values obtained at different measurement locations to produce an estimate of PWV spatial distribution. These distributions can be used both for validation of satellite data products (e.g., MODIS), but also to complement them. On one hand, MODIS provides high spatial resolution at a single moment in time, which can be used to improve interpolation between the MFRSRs locations. On the other hand, MFRSRs measurements, though being spatially more sparse, are made continuously in time and can be used to study the evolution of the WV field between the satellite overpass times.

[58] To illustrate the feasibility of using MFRSR network data for creation of 2D data sets comparable with the MODIS satellite water vapor product, we constructed a spatial distribution of columnar PWV from the MFRSR data obtained on 14 September 2000 at local noon (overpass time of Terra satellite) shown in Figure 14 (right). This distribution is in agreement with the corresponding map of the Terra MODIS PWV product (from NIR channels [*Gao and Kaufman*, 2003]) shown in Figure 14 (left). While lacking small-scale details (some of which are due to cloud contamination, especially in the southern part of the MODIS image), the MFRSR network provides an accurate spatial trend of PWV: increasing column amount from north-west to south-east of the site. This agreement is confirmed by the quantitative comparison shown in Figure 15 both for the exact MFRSR locations (left) and for all points in Figure 14 plots (right). The former expectedly demonstrates better agreement with MODIS, which values are smaller on average then the MFRSRs' by 0.2 cm with 0.2 cm standard deviation of the differences. Note, that only for 4 out of 18 MFRSR locations the differences with MODIS are outside the estimated 10% accuracy of the satellite retrievals. Comparison between MODIS data and the interpolated MFRSR values is not that good (0.3 cm mean difference, 0.4 cm standard deviation) largely because the above mentioned cloud contamination, which results in significantly underestimated PWV column values. Certainly, a single scene cannot provide a statistically significant validation of satellite product (moreover, that at the moment we do not have sufficient characterization of some of MFRSRs in the network). We leave a more detailed and extensive MFRSR-MODIS intercomparison for a future study, which

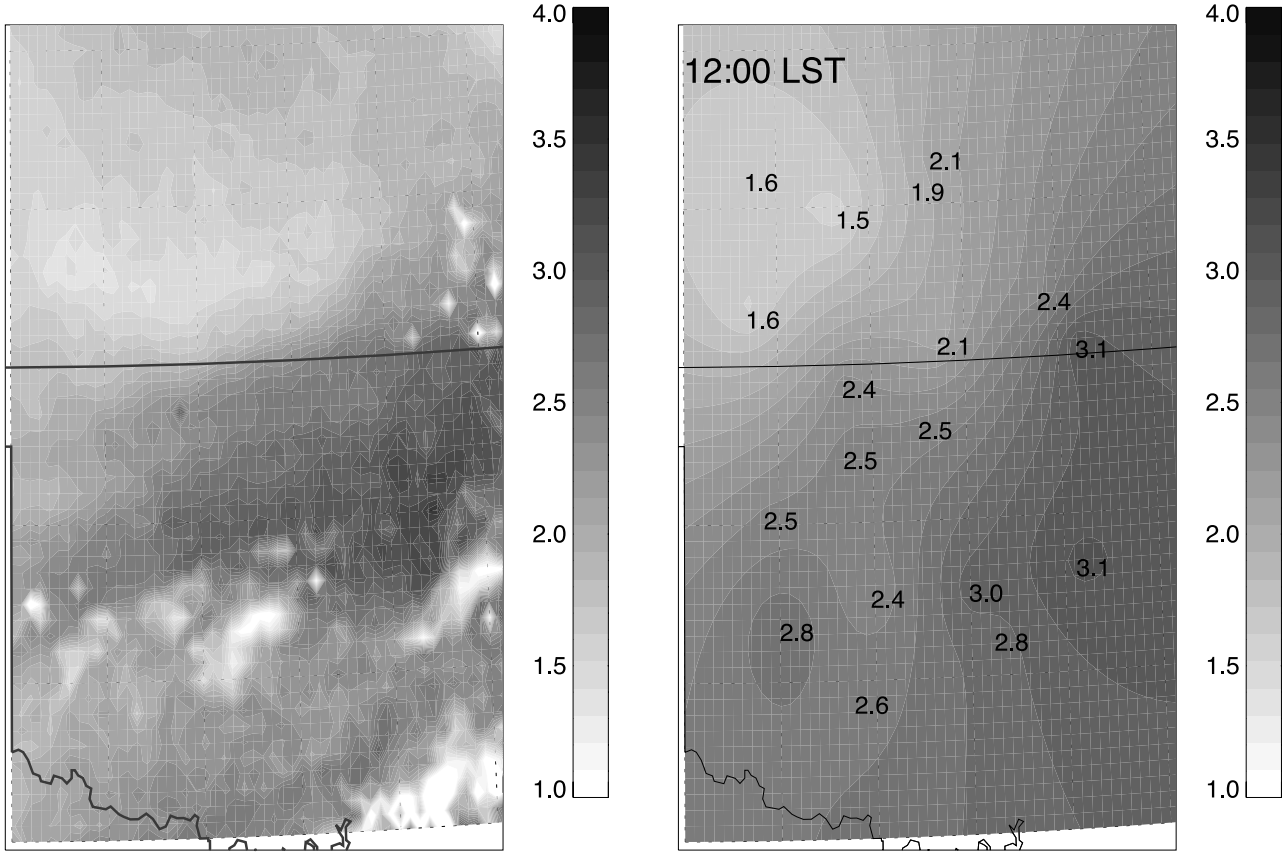

Figure 14. (left) MODIS Level 2 PWV product (from NIR channels) over the SGP site and (right) spatial structure obtained by interpolation of MFRSR network data from 12:00 noon on 14 September 2000. The numbers show the PWV column values (in centimeters) for each MFRSR location.

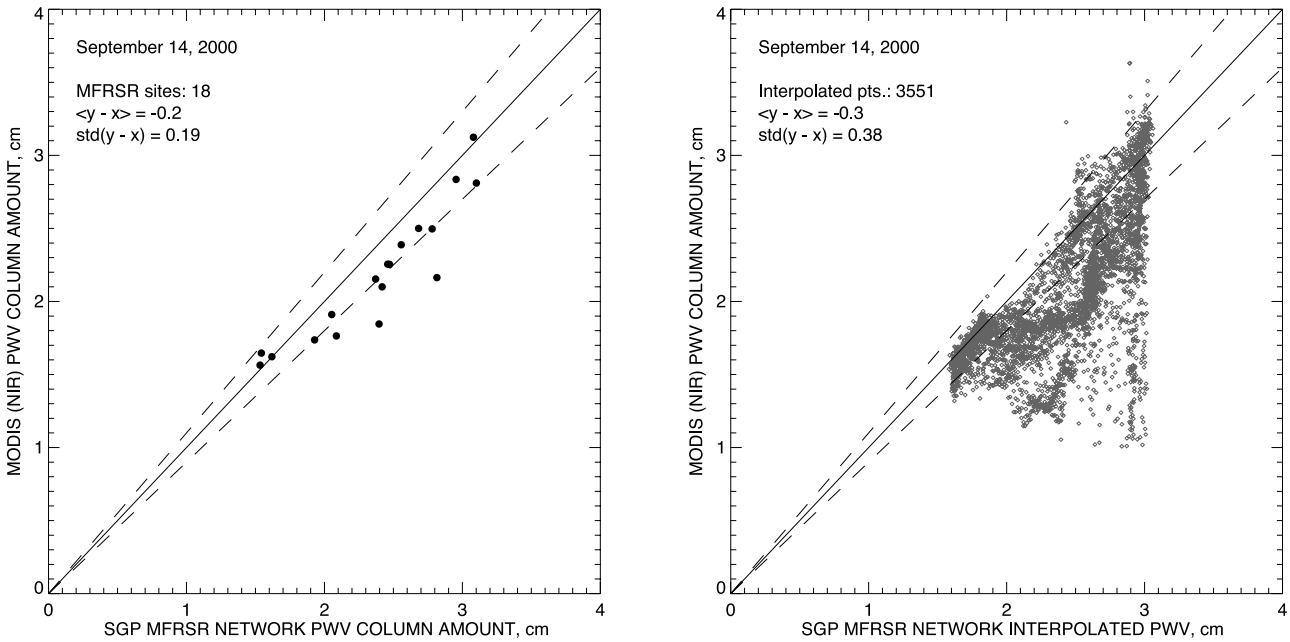

Figure 15. Comparison between the MODIS and MFRSR PWV retrievals from Figure 14: (left) for exact MFRSR sites locations and (right) for the 2D PWV field interpolated from the MFRSR network data. The dashed lines show ±10% MODIS error estimates.

should also include interpolation error estimates and comparison between different interpolation techniques.

5. Conclusions

[59] Measurements of precipitable water vapor content by solar radiometers are particularly useful for characterization of atmospheric state, since these instruments also provide simultaneous information on aerosol properties (AOD, particle size distribution). The MFRSRs have an additional advantage through the good spatial coverage they provide, especially in the US. The SGP site, in particular, provides a unique example of a dense regional MFRSR network capable of producing aerosol and PWV data sets characterizing both temporal and spatial variability of these atmospheric species. 2D slices of these data sets (for a specific moment of time) can be compared to satellite products (e.g., from MODIS, Figures 14 and 15) with help of a spatial interpolation technique, while evolution of these atmospheric fields can be tracked by MFRSR network beyond the time of satellite overpass. This ability is particularly significant for characterization of highly variable WV fields.

[60] Thus, development, testing and improvement of retrieval techniques, which allow for accurate determination of PWV column amount from MFRSR measurements is always important. Precipitable water vapor column amounts are determined from the direct normal irradiances in the 940 nm MFRSR spectral channel. The HITRAN 2004 spectral database was used to model the water vapor absorption. Our sensitivity study revealed a number of technical issues that can result in significant biases in PWV retrievals from MFRSR data. The most important factors include calibration of the 940-nm spectral channel, inadequate characterization of the instrument's spectral response, and uncertainties in current spectral absorption databases. Quantitative estimates of potential influence of these factors on retrievals at typical SGP's CF conditions are presented in Table 1.

[61] To make a practical estimate of the retrieval accuracy, the PWV column amounts derived from measurements by two SGP's CF MFRSRs (C1 and E13) were compared with each other and with a number of correlative measurements both by other solar radiometers (AERONET's CIMEL, AATS-6) and nonsolar instruments (microwave radiometers, GPS receiver). Data from the year 2000 (Figure 4) were chosen for intercomparisons. Some of these instruments (C1 MWR, AERONET, NPN GPS) routinely provide data throughout the year, while the other (ETL CSR, JPL WVR, and AATS-6) were deployed at SGP's CF during the Water Vapor IOP (WVIOP2000) from 18 September to 8 October 2000.

[62] We detected a 5% systematic disagreement between C1 and E13 MFRSRs during the year with C1 producing higher PWV column values (Figure 5, left). Our tests (Figure 6) lead us to conclude that these differences are mostly due to errors in calibration of one or both instruments. Note, that for typical atmospheric conditions at SGP the calibration constant for the 940 nm MFRSR channel cannot be reliably estimated from the data (using modified Langley plots [*Schmid et al.*, 2001]), thus we have to use laboratory calibrations.

[63] The MFRSR–MWR (MWRRET *phys* or *stat2* products, Figure 7) bias during both the whole year and the IOP period was quite large (6–10% for C1, 11–14% for E13). Analysis similar to that described above showed that the difference between the MFRSRs and the C1 MWR retrievals cannot be completely explained by MFRSR calibration error, and most likely includes contributions from other factors (such as error in MFRSR's spectral response function and/or in the absorption database used). Some disagreement with MWR may also be caused by differences in the field of view [*Michalsky et al.*, 1995], however this factor seems to be minor.

[64] Data from WVIOP2000 (Figure 9) shows better agreement within the groups of solar radiometers and of microwave radiometers than between these groups (Figure 16), with MWRs showing consistently positive biases relative the solar instruments. In particular, during this period (Figure 10) the bias of AATS-6 retrievals (using HITRAN 2000) relative to the C1 MFRSR data was −2%, while AERONET retrievals show 1% bias (−2.7% for the whole year data set). At the same time ETL CSR and JPL WVR show small biases (respectively 2 and −3%) relative to the C1 MWR (MWRRET *phys* product), while their comparison with the C1 MFRSR show much larger biases (respectively 4 and 7%). NPN GPS retrievals show 4.5% underestimation compared to MWRRET *stat2* data set during the IOP, while the bias for the yearlong data set is larger (7.5%), which makes them closer to C1 MFRSR with practically no bias (compared to 6% bias during the IOP).

[65] These estimates agree with conclusions by other authors. *Reagan et al.* [1995] report agreement between solar radiometer and microwave radiometer retrievals within 0.1 cm, yielding a percent difference generally within 10%. *Schmid et al.* [2001] provide a similar estimate, finding that with the [*Giver et al.*, 2000] spectroscopy the columnar PWV retrievals from the solar radiometers are 6–14% lower than the MWR results. *Kiedron et al.* [2001] report columnar PWV values measured in dry Arctic conditions by RSS (which does not have SRF-related problems) to be about 30% (0.25 mm) lower than the collocated MWR measurements. The HITRAN 1996 spectral absorption database corrected according to *Giver et al.* [2000] was used in that study. Comparisons of various PWV measurements at the SGP site with those by MWR during several WV IOPs were also presented by *Revercomb et al.* [2003].

[66] We see from Figure 16 that solar techniques show systematic underestimation relative to their nonsolar counterparts of the columnar PWV amounts larger than 2 cm. The same kind of disagreement is graphically shown in Figure 2 (bottom), where the curve of growth computed for the C1 MFRSR using HITRAN 2004 database has a different shape than the empirical curve based on the C1 MFRSR and the C1 MWR measurements. The same behavior is observed also in the data from other collocated MFRSR–MWR pairs at the SGP site, such as E13–C1, E16–B4 (located 6.2 km from each other), and E18–B5 ("B" denotes a boundary facility). This may indicate a rather general problem, since this disagreement cannot be explained by a MFRSR calibration error. MFRSR calibration adjustment may shift the empirical curve of growth up or down making it close to the theoretical curve at a short interval, however, it cannot eliminate the disagreement for all PWV values. The difference between the two curves becomes particularly noticeable for slant PWV column

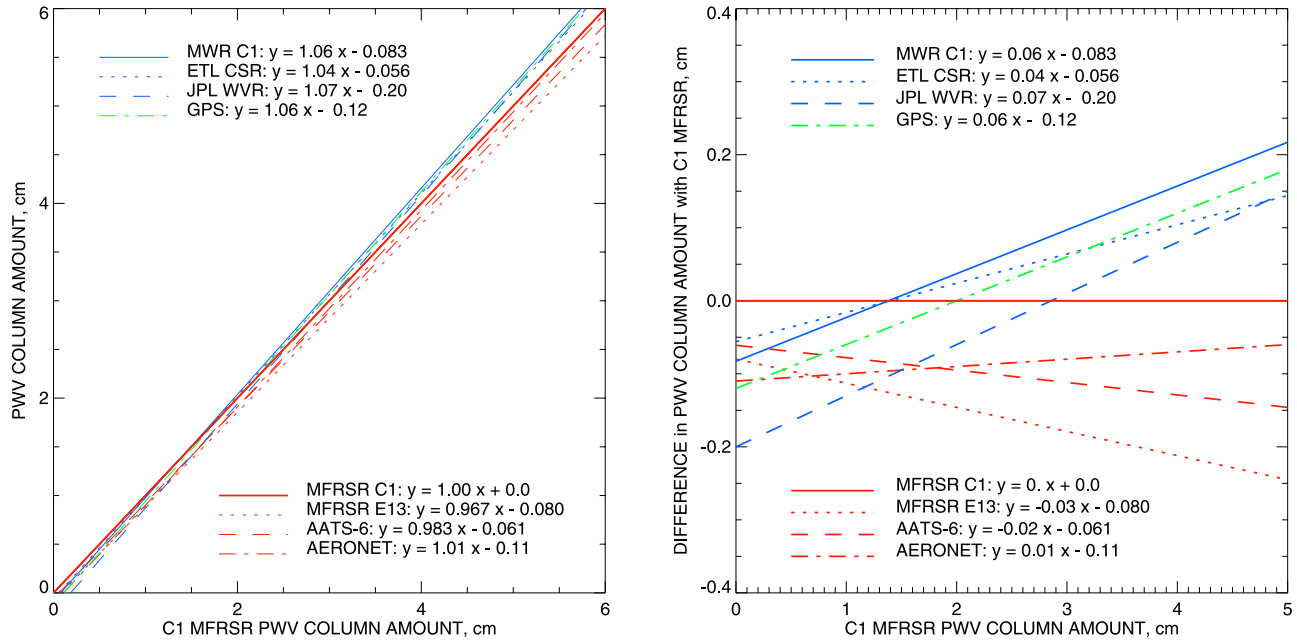

Figure 16. Summary of WVIOP2000 data intercomparison. (left) Regression lines for comparisons between PWV retrievals from C1 MFRSR and correlative measurements by other solar radiometers (E13 MFRSR, AERONET's CIMEL, and AATS-6, red lines), microwave radiometers (C1 MWR [MWRRET *phys*], ETL CSR, and JPL WVR, blue lines), and GPS WV sensor (green line). The 1-1 line is shown in red because formally it shows comparison of C1 MFRSR retrievals with themselves. (right) Difference between PWV measurements by the above instruments and those by C1 MFRSR based on the regression lines from the plot in the left.

amounts larger than 10 cm. While such large columnar PWV amounts are not typical for SGP, we can find a few cases, when possible error in the curve of growth shape leads to recognizable retrieval artifacts. One of such cases is presented in Figure 9 (bottom left) showing time series of PWV retrievals for 22 September 2000, when the PWV content was particularly high (around 4 cm). We see in this plot a simultaneous rapid decline in the retrievals from all 4 solar radiometers used in this study starting at about 15 h local time, while the data from the 3 MWRs and the GPS sensor show no specific change in behavior at this time. We think that the trend in the solar radiometer data is an artifact driven by increase in air mass (and, therefore, slant PWV OD) rather than an actual decrease in PWV content (the same behavior of MFRSR retrievals at large solar zenith angles can be also seen in the data from 23–24 June and 3 July 2000). This means, that the curves of growth used in the solar retrievals are too high in the range of large slant PWV column amounts (i.e., the empirical curve in Figure 2 (bottom) is closer to reality than the theoretical curve). We have shown that various technical problems can affect measurements of an individual solar radiometers. However, the three types of solar radiometers used in this study were independently characterized and calibrated by different science teams, that excludes errors in calibration or spectral response measurements as a possible cause of the systematic bias. This may indicate a need for further correction of spectral absorption databases and/or discovery of other factors affecting the retrievals. It is hard to come to terms with the fact that the old HITRAN 1996 database leads to a better agreement with MWR measurements in the large PWV column amount range than any later corrected versions.

[67] It is interesting, that *Sierk et al.* [2004] report the effect opposite to what we see in Figure 9 (bottom left). They observed a sharp increase in PWV column amount in the 940 nm band retrievals at large solar zenith angles, while (like in our case) GPS showed no systematic trend. This prompted them to advocate for the strong WV continuum in the CKD LBL model. Using this analogy, we can say that we need a "negative continuum" to reconcile our MFRSR retrievals with MWR and GPS data, since currently no WV continuum absorption is implied in our MFRSR data analysis. This qualitative disagreement between the study of *Sierk et al.* [2004] and this study (both using the same HITRAN 2004 database) indicates that a possibility of retrieval bias may come from uncertainties in the LBL models and the ways in which they are used. We suggest that a serious study should be performed comparing performance of different LBL models (especially at large PWV column amounts) to introduce more clarity into this subject.

[68] Like solar techniques, MWR measurements may also have unknown uncertainties. These measurements have shown very good agreement with Raman lidar PWV values, where the Raman lidar was calibrated with a chilled mirror hygrometer [*Revercomb et al.*, 2003; *Turner et al.*, 2007]. However, as solar radiometer retrievals, MWR data analysis also depends on spectral databases, which are also being adjusted. For example *Liljegren et al.* [2005] reported that replacing the value for the air-broadened half width of the 22-GHz water vapor line used in the absorption model of *Rosenkranz* [1998] with the 5% smaller half width from the

HITRAN compilation largely eliminated the systematic measurement error.

[69] It is well known that atmospheric WV is highly variable both temporary and spatially. High temporal variability of PWV column amount is seen in Figure 4, while Figure 14 (right) shows up to 50% differences in value between neighboring MFRSR locations (the average spacing of SGP network is 80 km). Our structure function analysis [cf. *Alexandrov et al.*, 2004b] applied to a large (one granule) MODIS PWV image (NIR channels) covering the northeastern US shows that on average the PWV column changes by $0.06\ r^{0.42}$ cm over the distance r (in km). This means on average a 0.5 cm change over 200 km distance. While more detailed quantitative characterization of WV variability will be a subject of our future studies, it is already evident that this variability may cause significant sampling errors in climatological estimates of PWV content derived from the spatially sparse network measurements or infrequent satellite overpass times. These errors may be comparable to, or even exceed, the measurement uncertainties.

[70] The above argument, however, does not eliminate the need for further development of PWV measurement techniques and reducing their uncertainties, especially systematic biases. We consider this study as a step in this direction and hope to expand on this work.

[71] The retrievals from MFRSR data used in this study are available from ARM Archive http://www.archive.arm.gov) as M. Alexandrov's PI data set.

[72] **Acknowledgments.** This research was supported by the Office of Biological and Environmental Research of the U.S. Department of Energy as part of the Atmospheric Radiation Measurement Program. We would like to thank S. J. Keihm for making JPL WVR measurements available, D. McIntosh and K. Longo for help with AATS-6 measurements, P. Kiedron and J. Michalsky for useful and stimulating discussions, and R. Wagener for his efforts to maintain AERONET site at SGP's Central Facility.

References

Ackerman, T. P., and G. Stokes (2003), The atmospheric radiation measurement program, *Phys. Today*, *56*, 38–45.

Albert, P., K. M. Smith, R. Bennartz, D. A. Newnham, and J. Fischer (2004), Satellite- and ground-based observations of atmospheric water vapor absorption in the 940 nm region, *J. Quant. Spectrosc. Radiat. Transfer*, *84*, 181–193.

Alexandrov, M., A. Lacis, B. Carlson, and B. Cairns (2002), Remote sensing of atmospheric aerosols and trace gases by means of multi-filter rotating shadow-band radiometer. part I: Retrieval algorithm, *J. Atmos. Sci.*, *59*, 524–543.

Alexandrov, M. D., A. Marshak, B. Cairns, A. A. Lacis, and B. E. Carlson (2004a), Automated cloud screening algorithm for MFRSR data, *Geophys. Res. Lett.*, *31*, L04118, doi:10.1029/2003GL019105.

Alexandrov, M., A. Marshak, B. Cairns, A. Lacis, and B. Carlson (2004b), Scaling properties of aerosol optical thickness fields retrieved from ground-based and satellite measurements, *J. Atmos. Sci.*, *61*, 1024–1039.

Alexandrov, M. D., P. Kiedron, J. J. Michalsky, G. Hodges, C. J. Flynn, and A. A. Lacis (2007), Optical depth measurements by shadow-band radiometers and their uncertainties, *Appl. Opt.*, *46*, 8027–8038.

Alexandrov, M. D., A. A. Lacis, B. E. Carlson, and B. Cairns (2008), Characterization of atmospheric aerosols using MFRSR measurements, *J. Geophys. Res.*, *113*, D08204, doi:10.1029/2007JD009388.

Augustine, J. A., G. B. Hodges, C. R. Cornwall, J. J. Michalsky, and C. I. Medina (2005), An update on SURFRAD—The GCOS Surface Radiation budget network for the continental United States, *J. Atmos. Ocean. Technol.*, *22*, 1460–1472.

Aumann, H. H., et al. (2003), AIRS/AMSU/HSB on the Aqua mission: Design, science objectives, data products, and processing system, *IEEE Trans. Geosci. Remote Sens.*, *41*, 253–264.

Beer, R. (2006), TES on the Aura Mission: Scientific objectives, measurements, and analysis overview, *IEEE Trans. Geosci. Remote Sens.*, *44*, 1102–1105.

Belmiloud, D., R. Schermaul, K. M. Smith, N. F. Zobov, J. W. Brault, R. C. M. Learner, D. A. Newnham, and J. Tennyson (2000), New studies of the visible and near-infrared absorption by water vapor and some problems with the HITRAN database, *Geophys. Res. Lett.*, *27*, 3703–3706.

Bigelow, D. S., J. R. Slusser, A. F. Beaubien, and J. H. Gibson (1998), The USDA ultraviolet radiation monitoring program, *Bull. Am. Meteorol. Soc.*, *79*, 601–615.

Brown, L. R., R. A. Toth, and M. Dulick (2002), Empirical line parameters of $H_2^{16}O$ near 0.94 μm: Positions, intensities and air-broadening coefficients, *J. Mol. Spectrosc.*, *212*, 57–82.

Bruegge, C. J., J. E. Conel, R. O. Green, J. S. Margolis, R. G. Holm, and G. Toon (1992), Water vapor column abundance retrievals during FIFE, *J. Geophys. Res.*, *97*, 18,759–18,768.

Cachorro, V. E., P. Utrillas, R. Vergaz, P. Duran, A. M. de Frutos, and J. A. Martinez-Lozano (1998), Determination of the atmospheric-water-vapor content in the 940-nm absorption band by use of moderate spectral-resolution measurements of direct solar irradiance, *Appl. Opt.*, *37*, 4678–4689.

Cimini, D., E. R. Westwater, Y. Han, and S. J. Keihm (2003), Accuracy of ground-based microwave radiometer and balloon-borne measurements during the WVIOP2000 field experiment, *IEEE Trans. Geosci. Remote Sens.*, *41*, 2605–2615.

Clough, S. A., F. X. Kneizys, and R. W. Davies (1989), Line shape and the water continuum, *Atmos. Res.*, *23*, 229–241.

Clough, S. A., M. W. Shephard, E. J. Mlawer, J. S. Delamere, M. J. Iacono, K. Cady-Pereira, S. Boukabara, and P. D. Brown (2005), Atmospheric radiative transfer modeling: A summary of the AER codes, *J. Quant. Spectrosc. Radiat. Transfer*, *91*, 233–244.

Collins, W. D., et al. (2006), Radiative forcing by well-mixed greenhouse gases: Estimates from climate models in the Intergovernmental Panel on Climate Change (IPCC) Fourth Assessment Report (AR4), *J. Geophys. Res.*, *111*, D14317, doi:10.1029/2005JD006713.

Fang, P., M. Bevis, Y. Bock, S. Gutman, and D. Wolfe (1998), GPS meteorology: Reducing systematic errors in geodetic estimates for zenith delay, *Geophys. Res. Lett.*, *25*, 3583–3586.

Fowle, F. E. (1912), The spectroscopic determination of aqueous vapor, *Astrophys. J.*, *35*, 149–162.

Fowle, F. E. (1915), The transparency of aqueous vapor, *Astrophys. J.*, *42*, 394–411.

Gao, B.-C., and Y. J. Kaufman (2003), Water vapor retrievals using moderate resolution imaging spectroradiometer (MODIS) near-infrared channels, *J. Geophys. Res.*, *108*(D13), 4389, doi:10.1029/2002JD003023.

Gates, D. M., and W. J. Harrop (1963), Infrared transmission of the atmosphere to solar radiation, *Appl. Opt.*, *2*, 887–898.

Giver, L. P., C. Chackerian Jr., and P. Varanasi (2000), Visible and near-infrared $H_2^{16}O$ line intensity corrections for Hitran-96, *J. Quant. Spectrosc. Radiat. Transfer*, *66*, 101–105.

Goody, R. M. (1964), *Atmospheric Radiation I. Theoretical Basis*, 436 pp., Oxford Univ. Press, New York.

Gordon, I. E., L. S. Rothman, R. R. Gamache, D. Jacquemart, C. Boone, P. F. Bernath, M. W. Shephard, J. S. Delamere, and S. A. Clough (2007), Current updates of the water-vapor line list in HITRAN: A new Diet for air-broadened half-widths, *J. Quant. Spectrosc. Radiat. Transfer*, *108*, 389–402.

Gutman, S. I., S. R. Sahm, S. G. Benjamin, B. E. Schwartz, K. L. Holub, J. Q. Stewart, and T. L. Smith (2004), Rapid retrieval and assimilation of ground based GPS precipitable water observations at the NOAA forecast systems laboratory: Impact on weather forecasts, *J. Meterol. Soc. Jpn.*, *82*, 351–360.

Halthore, R. N., T. F. Eck, B. N. Holben, and B. L. Markham (1997), Sun photometric measurements of atmospheric water vapor column abundance in the 940-nm band, *J. Geophys. Res.*, *102*, 4343–4352.

Han, Y., and E. R. Westwater (2000), Analysis and improvement of tipping calibration for ground-based microwave radiometers, *IEEE Trans. Geosci. Remote Sens.*, *38*, 1260–1277.

Hansen, J. E., and L. D. Travis (1974), Light scattering in planetary atmospheres, *Space Sci. Rev.*, *16*, 527–610.

Harrison, L., J. Michalsky, and J. Berndt (1994), Automated multifilter shadow-band radiometer: Instrument for optical depth and radiation measurement, *Appl. Opt.*, *33*, 5118–5125.

Harrison, L., P. Kiedron, J. Berndt, and J. Schlemmer (2003), Extraterrestrial solar spectrum 360–1050 nm from rotating shadowband spectroradiometer measurements at the Southern Great Plains (ARM) site, *J. Geophys. Res.*, *108*(D14), 4424, doi:10.1029/2001JD001311.

Holben, B. N., et al. (1998), AERONET—A federated instrument network and data archive for aerosol characterization, *Remote Sens. Environ.*, *66*, 1–16.

Ingold, T., B. Schmid, C. Matzler, P. Demoulin, and N. Kampfer (2000), Modeled and empirical approaches for retrieving columnar water vapor

from solar transmittance measurements in the 0.72, 0.82, and 0.94 μm absorption bands, *J. Geophys. Res.*, *105*, 24,327–24,343.

Kasten, F. (1965), A new table and approximation formula for the relative optical air mass, *Arch. Meteorol. Geophys. Bioklimatol. Ser. B*, *14*, 206–223.

Kasten, F., and A. T. Young (1989), Revised optical air mass tables and approximation formula, *Appl. Opt.*, *28*, 4735–4738.

Kaufman, Y. J., D. Tanre, L. A. Remer, E. Vermote, A. Chu, and B. N. Holben (1997), Operational remote sensing of tropospheric aerosol over land from EOS moderate resolution imaging spectroradiometer, *J. Geophys. Res.*, *102*, 17,051–17,067.

Kiedron, P. W., J. J. Michalsky, J. L. Berndt, and L. C. Harrison (1999), Comparison of spectral irradiance standards used to calibrate shortwave radiometers and spectroradiometers, *Appl. Opt.*, *38*, 2432–2439.

Kiedron, P., J. Michalsky, B. Schmid, D. Slater, J. Berndt, L. Harrison, P. Racette, E. Westwater, and Y. Han (2001), A robust retrieval of water vapor column in dry Arctic conditions using the rotating shadowband spectroradiometer, *J. Geophys. Res.*, *106*, 24,007–24,016.

Kiedron, P., J. Berndt, J. Michalsky, and L. Harrison (2003), Column water vapor from diffuse irradiance, *Geophys. Res. Lett.*, *30*(11), 1565, doi:10.1029/2003GL016874.

Kneizys, F. X., E. P. Shettle, L. W. Abreu, J. H. Chetwynd, G. P. Anderson, W. O. Gallery, J. E. A. Selby, and S. A. Clough (1988), User's guide to LOWTRAN 7, *Environ., Res. Pap., 1010*, *AFGL Tech. Rep. AFGL-TR-88-0177*, U.S. Air Force Geophys. Lab., Mass.

Koepke, P., and H. Quenzel (1978), Water vapor: Spectral transmission at wavelength between 0.7 μm and 1 μm, *Appl. Opt.*, *17*, 2114–2118.

Lacis, A. A., and V. Oinas (1991), A description of the correlated *k* distribution method for modeling nongray gaseous absorption, thermal emission, and multiple-scattering in vertically inhomogeneous atmospheres, *J. Geophys. Res.*, *96*, 9027–9063.

Liljegren, J. C., and B. M. Lesht (1996), Measurements of integrated water vapor and cloud liquid water from microwave radiometers at the DOE ARM cloud and radiation testbed in the U. S. Southern Great Plains, in *Proc. IGARSS '96*, pp. 1675–1677, IEEE, Lincoln, Nebr.

Liljegren, J. C., E. E. Clothiaux, G. G. Mace, S. Kato, and X. Dong (2001), A new retrieval for cloud liquid water path using a ground-based microwave radiometer and measurements of cloud temperature, *J. Geophys. Res.*, *106*, 14,485–14,500.

Liljegren, J. C., S. A. Boukabara, K. Cady-Pereira, and S. A. Clough (2005), The effect of the half-width of the 22-GHz water vapor line on retrievals of temperature and water vapor profiles with a 12-channel microwave radiometer, *IEEE Trans. Geosci. Remote Sens.*, *43*, 1102–1108.

Livingston, J. M., et al. (2005), Interactive comment on "Retrieval of ozone column content from airborne Sun photometer measurements during SOLVE II: Comparison with coincident satellite and aircraft measurements" by J. M. Livingston et al., *Atmos. Chem. Phys. Discuss.*, *5*, S1172–S1178.

Livingston, J., et al. (2007), Comparison of water vapor measurements by airborne Sun photometer and near-coincident in situ and satellite sensors during INTEX/ITCT 2004, *J. Geophys. Res.*, *112*, D12S16, doi:10.1029/2006JD007733.

Lyapustin, A. I. (2005), Radiative transfer code SHARM for atmospheric and terrestrial applications, *Appl. Opt.*, *44*, 7764–7772.

Matsumoto, T., P. Russell, C. Mina, W. Van Ark, and V. Banta (1987), Airborne tracking Sunphotometer, *J. Atmos. Ocean. Technol.*, *4*, 336–339.

Mavromatakis, F., C. A. Gueymard, and Y. Franghiadakis (2007), Technical note: Improved total atmospheric water vapour amount determination from near-infrared filter measurements with sun photometers, *Atmos. Chem. Phys.*, *7*, 4613–4623.

Michalsky, J. J., J. C. Liljegren, and L. C. Harrison (1995), A comparison of sunphotometer derivations of total column water vapor and ozone to standard measures of same at the Southern Great Plains atmospheric radiation measurement site, *J. Geophys. Res.*, *100*, 25,995–26,003.

Michalsky, J. J., J. A. Schlemmer, W. E. Berkheiser, J. L. Berndt, L. C. Harrison, N. S. Laulainen, N. R. Larson, and J. C. Barnard (2001a), Multiyear measurements of aerosol optical depth in the atmospheric radiation measurement and quantitative links programs, *J. Geophys. Res.*, *106*, 12,099–12,107.

Michalsky, J. J., Q. Min, P. W. Kiedron, D. W. Slater, and J. C. Barnard (2001b), A differential technique to retrieve column water vapor using sun radiometry, *J. Geophys. Res.*, *106*, 17,433–17,442.

Mikhail, E. M. (1976), *Observations and Least Squares*, 497 pp., IEP-Dunn-Donnelly, New York.

Mitchell, R. M., and B. W. Forgan (2003), Aerosol measurement in the Australian Outback: Intercomparison of Sun photometers, *J. Atmos. Ocean. Technol.*, *20*, 54–66.

Moskalenko, N. I. (1969), The spectral transmission function in the bands of water vapor, O_3, N_2O and N_2 atmospheric components, *Izv. Akad. Sci. USSR Atmos. Oceanic Phys.*, *5*, 1178.

Ohmura, A., et al. (1998), Baseline surface radiation network (BSRN/WCRP): New precision radiometry for climate research, *Bull. Am. Meteorol. Soc.*, *79*, 2115–2136.

Pitts, D. E., W. McAllum, and A. E. Dillinger (1974), Measurement of atmospheric precipitable water using a solar radiometer, *NASA Tech. Memo. X-58129*, NASA L. B. Johnson Space Cent., Houston, Tex.

Pitts, D. E., W. McAllum, M. Heidt, K. Jeske, J. T. Lee, D. DeMonbrun, A. Morgan, and J. Potter (1977), Temporal variations in atmospheric water vapor and aerosol optical depth determined by remote sensing, *J. Appl. Meteorol.*, *16*, 1312–1321.

Plana-Fattori, A., M. Legrand, D. Tanre, C. Devaux, A. Vermeulen, and P. Dubuisson (1998), Estimating the atmospheric water vapor content from Sun photometer measurements, *J. Appl. Meteorol.*, *37*, 790–804.

Plana-Fattori, A., P. Dubuisson, B. A. Fomin, and M. de Paula Correa (2004), Estimating the atmospheric water vapor content from multi-filter rotating shadow-band radiometry at Sao Paulo, Brazil, *Atmos. Res.*, *71*, 171–192.

Reagan, J., K. Thome, B. Herman, and R. Gall (1987a), Water vapor measurements in the 0.94 micron absorption band: Calibration, measurements, and data applications, in *Proc. Int. Geoscience and Remote Sensing '87 Symposium, Ann Arbor, Michigan, IEEE*, pp. 63–67.

Reagan, J. A., P. A. Pilewskie, I. C. Scott-Fleming, B. M. Herman, and A. Ben-David (1987b), Extrapolation of Earth-based solar irradiance measurements to exoatmospheric levels for broad-band and selected absorption-band observations, *IEEE Trans. Geosci. Remote Sens.*, *25*, 647–653.

Reagan, J., K. Thome, B. Herman, R. Stone, J. Deluisi, and J. Snider (1995), A comparison of columnar water-vapor retrievals obtained with near-IR solar radiometer and microwave radiometer measurements, *J. Appl. Meteorol.*, *34*, 1384–1391.

Reichert, L., M. D. Andres Hernandez, J. P. Burrows, A. B. Tikhomirov, K. M. Firsov, and I. V. Ptashnik (2007), First CRDS-measurements of water vapour continuum in the 940 nm absorption band, *J. Quant. Spectrosc. Radiat. Transfer*, *105*, 303–311.

Revercomb, H. E., et al. (2003), The ARM program's water vapor intensive observation periods, overview, initial accomplishments, and future challenges, *Bull. Am. Meteorol. Soc.*, *84*, 217–236.

Rosenkranz, P. W. (1998), Water vapor continuum absorption: A comparison of measurements and models, *Radio Sci.*, *33*, 919–928.

Rothman, L. S., et al. (2005), The HITRAN 2004 molecular spectroscopic database, *J. Quant. Spectrosc. Radiat. Transfer*, *96*, 139–204.

Schermaul, R., R. C. M. Learner, D. A. Newnham, R. G. Williams, J. Ballard, N. F. Zobov, D. Belmiloud, and J. Tennyson (2001a), The water vapor spectrum in the region 8600–15 000 cm^{-1}: Experimental and theoretical studies for a new spectral line database. I: Laboratory measurements, *J. Mol. Spectrosc.*, *208*, 32–42.

Schermaul, R., R. C. M. Learner, D. A. Newnham, J. Ballard, N. F. Zobov, D. Belmiloud, and J. Tennyson (2001b), The water vapor spectrum in the region 8600–15 000 cm^{-1}: Experimental and theoretical studies for a new spectral line database. II: Linelist construction, *J. Mol. Spectrosc.*, *208*, 43–50.

Schmid, B., K. J. Thome, P. Demoulin, R. Peter, C. Matzler, and J. Sekler (1996), Comparison of modeled and empirical approaches for retrieving columnar water vapor from solar transmittance measurements in the 0.94-μm region, *J. Geophys. Res.*, *101*, 9345–9358.

Schmid, B., P. R. Spyak, S. F. Biggar, C. Wehrli, J. Sekler, T. Ingold, C. Matzler, and N. Kampfer (1998), Evaluation of the applicability of solar and lamp radiometric calibrations of a precision Sun photometer operating between 300 and 1025 nm, *Appl. Opt.*, *37*, 3923–3941.

Schmid, B., et al. (2001), Comparison of columnar water-vapor measurements from solar transmittance methods, *Appl. Opt.*, *40*, 1886–1896.

Schmid, B., et al. (2003), Column closure studies of lower tropospheric aerosol and water vapor during ACE-Asia using airborne Sun photometer and airborne in situ and ship-based lidar measurements, *J. Geophys. Res.*, *108*(D23), 8656, doi:10.1029/2002JD003361.

Shiobara, M., J. D. Spinhirne, A. Uchiyama, and S. Asano (1996), Optical depth measurements of aerosol, cloud, and water vapor using Sun photometers during FIRE Cirrus IFO II, *J. Appl. Meteorol.*, *35*, 36–46.

Sierk, B., S. Solomon, J. S. Daniel, R. W. Portmann, S. I. Gutman, A. O. Langford, C. S. Eubank, E. G. Dutton, and K. H. Holub (2004), Field measurements of water vapor continuum absorption in the visible and near-infrared, *J. Geophys. Res.*, *109*, D08307, doi:10.1029/2003JD003586.

Smirnov, A., B. N. Holben, T. F. Eck, O. Dubovik, and I. Slutsker (2000), Cloud screening and quality control algorithms for the AERONET database, *Remote Sens. Environ.*, *73*, 337–349.

Smirnov, A., B. N. Holben, A. Lyapustin, I. Slutsker, and T. F. Eck (2004), AERONET processing algorithms refinement, paper presented at AERONET Workshop, El Arenosillo, Spain, 10–14 May.

Smith, T. L., S. G. Benjamin, S. I. Gutman, and S. R. Sahm (2007), Forecast impact from assimilation of GPS-IPW observations into the rapid update cycle, *Mon. Weather Rev.*, *135*, 2914–2930.

Teillet, P. M. (1990), Rayleigh optical depth comparisons from various sources, *Appl. Opt.*, *29*, 1897–1900.

Thome, K., B. Herman, and J. Reagan (1992), Determination of precipitable water from solar transmission, *J. Appl. Meteorol.*, *31*, 157,165.

Thome, K. J., M. W. Smith, J. M. Palmer, and J. A. Reagan (1994), Three-channel solar radiometer for the determination of atmospheric columnar water vapor, *Appl. Opt.*, *33*, 5811–5819.

Tipping, R. H., and Q. Ma (1995), Theory of the water-vapor continuumand validations, *Atmos. Res.*, *36*, 69–94.

Tobin, D. C., H. E. Revercomb, R. O. Knuteson, B. M. Lesht, L. L. Strow, S. E. Hannon, W. F. Feltz, L. A. Moy, E. J. Fetzer, and T. S. Cress (2006), Atmospheric radiation measurement site atmospheric state best estimates for Atmospheric Infrared Sounder temperature and water vapor retrieval validation, *J. Geophys. Res.*, *111*, D09S14, doi:10.1029/2005JD006103.

Tolchenov, R. N., M. Tanaka, J. Tennyson, N. F. Zobov, S. V. Shirin, O. L. Polyansky, and A. N. Maurellis (2003), Water line intensities in the near-infrared and visible, *J. Quant. Spectrosc. Radiat. Transfer*, *82*, 151–163.

Turner, D. D., S. A. Clough, J. C. Liljegren, E. E. Clothiaux, K. Cady-Pereira, and K. L. Gaustad (2007), Retrieving liquid water path and precipitable water vapor from atmospheric radiation measurement (ARM) microwave radiometers, *IEEE Trans. Geosci. Remote Sens.*, *45*, 3680–3690.

Villevalde, Y. V., V. M. Volgin, and K. S. Shifrin (1988), The accuracy of aerosol optical depth spectral behaviour determination with filter solar radiation measurements, *Sov. Meteorol. Hydrol., Engl. Transl.*, *6*, 116–120.

Vogelmann, A. M., V. Ramanathan, W. C. Conant, and W. E. Hunter (1998), Observational constraints on non-Lorentzian continuum effects in the near-infrared solar spectrum using ARM ARESE data, *J. Quant. Spectrosc. Radiat. Transfer*, *60*, 231–246.

Westwater, E. R. (1993), Ground-based microwave remote sensing of meteorological variables, in *Atmospheric Remote Sensing by Microwave Radiometry*, edited by M. A. Janssen, pp. 145–213, John Wiley, New York.

Wolfe, D. E., and S. I. Gutman (2000), Developing an operational, surface-based, GPS, water vapor observing system for NOAA: Network design and results, *J. Atmos. Ocean. Technol.*, *17*, 426–439.

World Climate Research Programme Baseline Surface Radiation Network (2001), Report of the sixth BSRN science and review workshop (Melbourne, Australia, 1–5 May 2000), *WCRP Informal Report No. 17/2001*, World Climate Research Programme, World Meteorol. Organ., Geneva.

M. D. Alexandrov, Department of Applied Physics and Applied Mathematics, Columbia University and NASA Goddard Institute for Space Studies, 2880 Broadway, New York, NY 10025, USA. (malexandrov@giss.nasa.gov)

B. Cairns and A. A. Lacis, NASA Goddard Institute for Space Studies, 2800 Broadway, New York, NY 10025, USA.

J. Eilers, NASA Ames Research Center, MS 245-5, Building 245, Room 6, Moffett Field, CA 94035, USA.

S. I. Gutman, NOAA Earth System Research Laboratory, 325 Broadway R/GSD7, Boulder, CO 80305-3328, USA.

V. Oinas, Sigma Space Partners LLC, 280 Broadway, New York, NY 10025, USA.

B. Schmid, Atmospheric Science and Global Change Division, Pacific Northwest National Laboratory, MSIN: K9-24, 902 Battelle Boulevard, P.O. Box 999, Richland, WA 99352, USA.

A. Smirnov, Science Systems and Applications, Inc., NASA Goddard Space Flight Center, Code 614.4, Building 33, Greenbelt, MD 20771, USA.

D. D. Turner, Space Science and Engineering Center, University of Wisconsin, 1225 W. Dayton Street, Madison, WI 53706, USA.

E. R. Westwater, NOAA-CU Center for Environmental Technology and Cooperative Institute for Research in Environmental Science, Department of Electrical and Computer Engineering, University of Colorado, 425 UCB-ECOT 249, Boulder, CO 80309-0425, USA.